Title: Interaction of Angio-associated Migratory Cell Protein with the TPα and TPβ isoforms of the human Thromboxane A_2 receptor.

Running Title: AAMP interacts with TPα and TPβ.

Helen M. Reid*, Katarina Wikström*, David J. Kavanagh, Eamon P. Mulvaney and B. Therese Kinsella†

School of Biomolecular and Biomedical Sciences, Conway Institute of Biomolecular and Biomedical Research, University College Dublin, Belfield, Dublin 4, Ireland.

* These authors contributed equally to this study.

†Corresponding author: Tel: 353-1-7166727; Fax 353-1-7166456;

Email: Therese.Kinsella@UCD.IE

Keywords

Thromboxane, receptor, angio-associated migratory cell protein, RhoA, cell migration, interactant, yeast two hybrid.

Abbreviations:

AAMP, angio-associated migratory cell protein; AoSMC, aortic smooth muscle cell; CoASMC, coronary artery smooth muscle cell; C-tail, carboxyl-terminal tail; FBS, foetal bovine serum; GPCR, G protein-coupled receptor; GST, glutathione-S-transferase; HA, hemagglutinin; HB, heparin binding; HEK, human embryonic kidney; *si*RNA, *small interfering* RNA; SMC, smooth muscle cells; TP, thromboxane A_2 receptor; TX, thromboxane; VEGF, vascular endothelial growth factor; WD-40, Trp Asp-enriched domain of 40 amino acids; Y2H, yeast two hybrid.

Synopsis

In humans, thromboxane (TX) A_2 signals through the TPα and TPβ isoforms of its G-protein coupled TXA_2 receptor (TP) to mediate a host of (patho)physiologic responses. Herein, angio-associated migratory cell protein (AAMP) was identified as a novel interacting partner of both TPα and TPβ through an interaction dependent on common (residues 312-328) and unique (residues 366-392 of TPβ) sequences within their carboxyl-terminal (C)-tail domains. While the interaction was constitutive in mammalian cells, agonist-stimulation of TPα/TPβ led to a transient dissociation of AAMP from immune complexes which coincided with a transient redistribution of AAMP from its localization in an intracellular fibrous network. Although the GTPase RhoA is a downstream effector of both AAMP and the TPs, AAMP did not influence TP-mediated RhoA or *vice versa*. *Small interfering* RNA (*si*RNA)-mediated disruption of AAMP expression decreased migration of primary human coronary artery smooth muscle cells (1° hCoASMCs). Moreover, *si*RNA-disruption of AAMP significantly impaired 1° hCoASMC migration in the presence of the TXA_2 mimetic U46619 but did not affect VEGF-mediated cell migration. Given their roles within the vasculature, the identification of a specific interaction between TPα/TPβ and AAMP is likely to have substantial functional implications for vascular pathologies in which they are both implicated.

Introduction

Angio-associated migratory cell protein (AAMP), initially identified during a search for motility-associated proteins [1], is predominantly expressed in cells with a migratory phenotype including vascular endothelial and smooth muscle cells, renal proximal tubular cells and activated T lymphocytes [2]. Expression of AAMP is elevated in invasive gastrointestinal stromal tumours [3] and in ductal carcinoma in situ (DCIS) of the breast, where it is viewed as a poor prognostic marker [4]. A recent study identified a direct interaction of AAMP with nucleotide-binding oligomerization domain containing 2 (Nod2), thereby also suggesting a possible role in the innate immune response [5].

AAMP is a WD-40 repeat-containing protein and is also predicted to contain two immunoglobulin (Ig)-like domains and a putative membrane association domain [1]. The WD-40 repeat motif is found in a wide range of proteins with diverse roles in signal transduction, transcriptional activation, cytoskeletal regulation and cell cycle control [6]. This myriad of functions stems from the ability of WD-40 repeat-containing proteins to act as adaptors/scaffolds in multi-protein complexes, largely due to their conserved structural organization into a β-propeller fold, with each of the WD-40 repeats arranged toroidally as the "blades" of the propeller [7]. Typically, WD-40 repeat-containing proteins contain 7 repeats, as in the case of the G-protein β subunit [8, 9], although proteins containing 4 – 16 repeats have been described [10, 11].

Evidence for a role for AAMP in cell migration is expanding. Treatment with an *anti*-AAMP antibody inhibits endothelial tube formation and cell migration [2, 12]. Smooth muscle cell (SMC) migratory potential is elevated upon over-expression of AAMP and inhibited by either neutralizing *anti*-AAMP antibody or *si*RNA-directed knockdown [13]. Interestingly, blockade of AAMP in SMCs led to a decrease in membrane translocation and possible activation of RhoA [13], the GTPase widely implicated in the reorganization of the actin cytoskeleton that accompanies SM contraction and/or cell migration [14]. In addition, that same study [13] demonstrated significant up-regulation of AAMP expression in SMCs associated with various experimental atherosclerotic and restenotic animal models, leading to the proposal that AAMP might contribute to the accompanying neo-intima thickening, possibly through its modulation of RhoA.

The prostanoid thromboxane (TX) A_2 plays a central role within the vasculature including its dynamic regulation of platelet activation status, SM contraction and possible modulation of SMC proliferation and/or migration [15-19]. Accordingly, aberrant TXA_2 signalling is widely implicated in a number of cardiovascular disorders including thrombosis, various hypertensions and in the progression of atherosclerosis and restenosis [20, 21] and, more recently, in certain neoplasms [22-24]. TXA_2 mediates its effects through the TXA_2 receptor (TP), a member of the G-protein coupled receptor (GPCR) superfamily, of which there are two distinct isoforms, termed TPα and TPβ, in humans and other primates but not in earlier species. TPα and TPβ are identical for their N-terminal 328 residues but differ exclusively within their carboxyl-terminal (C-tail) domains [25-28]. In humans, TPα and TPβ arise through alternative splicing of a common 1^o transcript but display distinct patterns of expression throughout the vasculature, being transcriptionally regulated by distinct promoters within the single TP gene [29-36].

Both TPα and TPβ show identical coupling to Gq/phospholipase (PL)Cβ and to G_{12}-mediated RhoA activation leading to Ca^{2+}-dependent and Ca^{2+}-independent responses, respectively, such as in platelets and SMCs [37, 38], but may differentially regulate other effectors including opposite coupling to adenylyl cyclase through G_s and G_i, respectively [39]. In studies investigating crosstalk of signalling between TXA_2 and the vasodilatory prostanoid prostacyclin (prostaglandin I_2), it was established that both Gq/PLCβ and G_{12}/RhoA signalling by TPα, but not TPβ, undergoes prostacyclin-induced desensitization involving direct cAMP-dependent protein kinase (PK) A phosphorylation of TPα at Ser^{328} within its unique C-tail domain [37, 38, 40]. In addition, both Gq/PLCβ and G_{12}/RhoA signalling by TPα, but not TPβ, is desensitized by the vasodilator nitric oxide (NO) involving direct NO/cGMP-dependent PKG phosphorylation of TPα at Ser^{329} also within its unique C-tail domain [37, 41]. The implication of the latter studies is that TPα may be the major TP isoform involved in vascular hemostasis, being subject to desensitization/inhibition of signalling by both prostacyclin and NO, while the role of TPβ in haemostasis is currently unknown. In addition to such differences in the patterns of desensitization of TPα and TPβ in response to heterologous agents including prostacyclin and NO, they are also subject to distinct differences in their mechanisms of agonist-induced or homologous desensitization whereby that of TPβ occurs through the classic GPCR kinase (GRK)-dependent mechanism while that of TPα occurs through a feedback mechanism involving PKC and PKG [42, 43]. Hence, whilst the significance of two receptor isoforms for TXA_2 in humans is unclear, there is substantial evidence that TPα and TPβ have distinct physiological roles, displaying critical differences in their patterns of expression and modes of regulation.

Aside from their classic interaction with heterotrimeric G-proteins, it is now well established that GPCRs may regulate an array of other cellular signalling events through their direct interaction with a wide range of proteins, known collectively as GPCR interacting proteins or GIPs [44, 45]. These interactions mediate diverse functions such as the regulation of T lymphocyte migration through interaction of the CCR5 and CXCR4 chemokine receptors with myosin heavy chain IIA [46] and the regulation of the recycling of the prostacyclin receptor through a direct interaction with Rab11a [47, 48]. In many cases, the intracellular carboxyl-terminal (C) tail of the GPCR has emerged as the critical binding domain for such interactions with various GIPs, largely due to its divergent sequence, structure and capacity to contain functionally distinct binding motifs [44, 45, 49].

In view of the critical structural and functional differences between the TPα and TPβ isoforms, the aim of the current study was to apply a two-hybrid screening approach to identify novel interacting partners, or GIPs, of TPα and/or TPβ whereby the C-tail domains, encoding sequences both common and unique to each isoform, were used as bait proteins during the primary high stringency screen. Herein, we report on the identification and characterization of a novel interaction between both TPα and TPβ with AAMP and explore the functional implications of that interaction.

Experimental

Materials.

The MATCHMAKER™ human kidney cDNA library, HY4043AH, and the plasmids pGBKT7 and pGBKT7:p53 encoding the GAL4 DBD alone or as a fusion with p53, were obtained from Clontech; pGEX-5X-1 and Glutathione-Sepharose 4B were from GE Healthcare; pCMVTag2A/B/C vectors and the Quikchange™ site-directed mutagenesis system were from Stratagene. The rabbit reticulocyte lysates *in vitro* transcription and translation system (TnT®) was from Promega. Effectene was from Qiagen; *anti*-FLAG© M2 monoclonal antibody (F3165), mouse monoclonal *anti*-FLAG horseradish peroxidise (HRP)-conjugate, protein-A-sepharose CL-4B, protein G-sepharose were from SigmaAldrich; *anti*-GST, *anti*-RhoA 26C4, anti-α-actinin (H2), HRP conjugated goat *anti*-mouse (400 µg/ml) and HRP conjugated goat *anti*-rabbit (400 µg/ml) were from Santa Cruz; affinity purified rabbit polyclonal *anti*-AAMP antibody was obtained from Strategic Diagnostics (Clone # 24430002); *anti*-HDJ2 (DNAJ protein) antibody from Neomarkers; *anti*-Myc (9B11) mouse monoclonal antibody was from Cell Signaling Technology; rat monoclonal 3F10 *anti*-hemagglutinin (HA)-HRP conjugated antibody (25 µg/ml) was from Roche; mouse monoclonal anti-HA-101R antibody (1 mg/ml) was obtained from Cambridge Biosciences; AlexaFluor488 goat *anti*-rabbit and AlexaFluor594 goat anti-mouse antibodies were from Molecular Probes. U46619 was obtained from Cayman Chemical Company. All oligonucleotides were synthesised by Sigma Genosys.

Expression plasmids.

The plasmids pGBKT7:TPα$^{312\text{-}343}$ and pGBKT7:TPβ$^{312\text{-}407}$ encoding the carboxyl-terminal (C)-tail domains of TPα (amino acid 312-343) and TPβ (amino acid 312-407) were amplified by PCR using pHM6:TPα and pHM6:TPβ as templates [38] and sub-cloned into the EcoR1/BamH1 site of the yeast bait vector pGBKT7 (Clontech) such that the inserts were c-Myc epitope tagged and in-frame with the DNA-binding domain (DBD) of the yeast GAL4 transcriptional regulator. Similarly, pGBKT7:TPα$^{329\text{-}343}$, pGBKT7:TPβ$^{329\text{-}407}$, pGBKT7:TPβ$^{312\text{-}392}$, pGBKT7:TPβ$^{312\text{-}366}$, pGBKT7:TPβ$^{329\text{-}392}$, pGBKT7:TPβ$^{329\text{-}366}$, pGBKT7:TPβ$^{353\text{-}392}$ and pGBKT7:TPβ$^{353\text{-}366}$ were generated by subcloning the respective PCR amplified fragments from pHM6:TPα and pHM6:TPβ in-frame into the EcoR1/BamH1 site of pGBKT7. The plasmids pGBKT7:TPβ$^{312\text{-}353}$ and pGBKT7:TPβ$^{329\text{-}353}$ were generated by Quickchange™ site-directed mutagenesis using pGBKT7:TPβ$^{312\text{-}407}$ and pGBKT7:TPβ$^{329\text{-}407}$ as templates, respectively, and customised mutator primers designed to convert codon 354 to a Stop codon. Plasmids pGEX-5X-1:TPα$^{312\text{-}343}$, pGEX-5X-1:TPα$^{329\text{-}343}$, pGEX-5X-1:TPβ$^{312\text{-}407}$ and pGEX-5X-1:TPβ$^{329\text{-}407}$ were generated by subcloning the respective regions from the corresponding pGBKT7:TPα/TPβ plasmids into the EcoR1/Sal1 sites of pGEX-5X-1, such that the fragments were cloned in-frame with glutathione-S-transferase (GST). The plasmids pGEX-5X-1:IC$^{A52\text{-}L70}$, pGEX-5X-1:IC$^{E129\text{-}E149}$ and pGEX-5X-1:IC$^{E221\text{-}E246}$ were generated by subcloning the respective PCR amplified fragments encoding amino acids 52-70, 129-149 and 221-246, corresponding to intracellular domains $(IC)_1$, IC_2 and IC_3, of TPα/TPβ, respectively into the EcoR1/Sal1 sites of pGEX-5X-1. The plasmids pCMVTag2b:AAMP$^{\Delta 348}$, pCMVTag2b:AAMP$^{\Delta 298}$, or pCMVTag2b:AAMP$^{\Delta 165}$ were generated by Quickchange™ site-directed mutagenesis using pCMVTag2b:AAMP^{WT} as template, and customised mutator primers designed to convert

codons 349, 299 and 166 of AAMP, respectively, to Stop codons. All plasmids were validated by DNA sequence analysis.

Yeast-two-hybrid screening and yeast matings.

All yeast protocols were standard procedures as previously described [48]. Briefly, the human kidney cDNA library, cloned in-frame with the activation domain of the yeast GAL4 transcriptional activator in the yeast prey plasmid pACT2 and pre-transformed into MATa *Saccharomyces cerevisiae* (*S.c*) Y187 was obtained from Clontech (3.5 X 10^6 independent clones; HY4034AH). All pGBKT7-based plasmids were transformed into the MATα *Saccharomyces cerevisiae* (*S.c*) AH109 strain. The pGBKT7-based bait plasmids and pACT2-based prey plasmids were mated with selection of diploids on synthetic double drop-out (DDO) media (SD/Leu$^-$, Trp$^-$). Positive interactions between bait and prey proteins were identified by expression of the *HIS3*, *ADE2* and *MEL1* reporter genes on quadruple drop-out (QDO) media (SD/Leu$^-$, Trp$^-$, His$^-$, Ade$^-$) and for the ability to cleave *X*-α-gal (5-bromo-4-chloro-3-indolyl-α-D-galactopyranoside), as measured by the filter lift assay of α-Galactosidase (α-Gal) activity. The scoring system used in the latter was based on the ability of 3 independent colonies selected from respective DDO media to produce blue (+) or white (-) colonies owing to expression of α-Gal activity where, as indicated in the figure legends, '+++' was used to indicate that cells developed blue colour within 30 min of assay and '-' indicates cells remain white over the period of the assay (4 hr).

For analysis of protein expression in *S.c*. AH109 (pGBKT7) bait or *S.c* Y187 (pACT2) prey transformants, protein was extracted, resolved by SDS-PAGE, and screened by western blot analysis using *anti*-Myc (9B11), with chemiluminescence detection [38].

Cell culture and transfections.

Human embryonic kidney (HEK) 293 cells were obtained from the American Type Culture Collection and grown in minimal essential medium (MEM) containing 10 % foetal bovine serum (FBS). Routinely, approximately 48 hours prior to transfection, cells were plated at a density of 2 x 10^6 cells/10 cm dish in 8 ml media. Thereafter, cells were transiently transfected with 0.5 μg of pADVA [50] and 2 μg of the pCMVTag2b-based vectors by Effectene transfection, as per the manufacturers' instructions. Transiently transfected cells were harvested 48 hr post-transfection, unless otherwise stated. HEK.TPα, HEK.TPβ cells stably over-expressing haemagglutinin (HA)-tagged forms of TPα, TPβ, respectively, have been previously described [37]. HEK.β-galactosidase (HEK.β-Gal) cells stably overexpressing the HA-tagged β-galactosidase (β-Gal) were generated essentially as previously described [51, 52]. Human erythroleukemic (HEL) 92.1.7 cells were cultured in RPMI 1640, 10 % foetal bovine serum (FBS). EA.hy 926 cells were obtained from the Tissue Culture Facility at UNC Lineberger Comprehensive Cancer Center, North Carolina and were grown in Dulbecco's modified Eagle's medium (DMEM) containing 10 % FBS [53]. Primary (1°) human aortic smooth muscle cells (1° hCoASMCs) were from Cascade Biologics and routinely grown in Smooth Muscle Cell Growth Medium 2 supplemented with 0.5 ng/ml epidermal growth factor, 2 ng/ml

basic fibroblast growth factor, 5 µg/ml insulin and 5 % FBS (Promocell GmBH). 1° human umbilical vein endothelial cells (HUVECs), from Lonza (IRT9-048-0904D), were routinely cultured in M199 media (Sigma-Aldrich) supplemented with 0.4 % (v/v) Endothelial Cell Growth Supplement/Heparin (ECGS/H; Promocell GmBH), 20 % (v/v) FBS and 0.2 % (v/v) L-glutamine. 1° hCoASMC and 1° HUVECs were routinely used between passages 2 - 8. All mammalian cells were grown at 37 °C in a humid environment with 5 % CO_2 and confirmed to be mycoplasma free.

Glutathione-S-transferase pull-down assay.

E.coli Rossetta 2 (DE3) transformed with the plasmids pGEX-5X-1:TPα$^{312-343}$, pGEX-5X-1:TPα$^{329-343}$, pGEX-5X-1:TPβ$^{312-407}$ and pGEX-5X-1:TPβ$^{329-407}$ were grown in LB media supplemented with ampicillin (50 µg/ml) and chloramphenicol (34 µg/ml) until a optical density (OD) at 600 nm of 0.8 was achieved. Thereafter, cultures were supplemented with 0.25 mM isopropyl β-D-1-thiogalactopyranoside (IPTG) and incubated for 1 hr at 4 °C to induce recombinant protein expression. Following induction, cells were harvested by centrifugation at 5,000 g for 10 min at 4 °C and the resulting pellets lysed by sonication (8 cycles of 15 s with 1 min intervals at 15 microns) in lysis buffer (150 mM NaCl, 5 mM $MgCl_2$, 1 % Triton-X-100, 50 mM Tris-Cl, pH7.5, 1 mM DTT, 10 µg/ml aprotinin, 10 µg/ml leupeptin and 0.1 mM PMSF). Cellular debris was removed by centrifugation as described and the supernatant(s) were incubated at room temperature for 30-60 min with 1 ml 50 % slurry of Glutathione-Sepharose 4B beads, previously equilibrated with 5 ml wash buffer (50 mM Tris-Cl, pH 7.5, 150 mM NaCl, 5 mM $MgCl_2$, 0.5 % Triton-X-100, 1 mM DTT, 1 µg/ml aprotinin, 1 µg/ml leupeptin and 0.1 mM PMSF). Thereafter, the purified recombinant GST proteins were washed six times in wash buffer.

HA.AAMP$^{308-434}$ was translated from the PCR amplified product encoding the T7 promoter sequence, optimal translation initiation site (GAG CCA CCA TG), HA-epitope tag and amino acids 308-434 of AAMP using the TNT® T7 coupled *in vitro* transcription/translation system (Promega). Per GST pull-down, 10 µg each of the purified GST.TPα$^{312-343}$, GST.TPα$^{329-343}$, GST.TPβ$^{312-407}$, GST.TPβ$^{329-407}$ and GST bound to Glutathione Sepharose 4B beads were pre-equilibrated in pull-down buffer A (20 mM HEPES, pH 7.4, 100 mM NaCl, 2 mM $MgCl_2$, 0.1 % Triton-X-100) supplemented with 1 % BSA for 30-60 min prior to washing in three changes of buffer A. Thereafter, beads containing 4 µg of the respective GST-fusion protein were incubated with the *in vitro* translated product HA.AAMP$^{308-434}$ (2 µl) at room temperature for 2 hr with rotation. Following three washes in buffer A, beads were resuspended in immunoprecipitation (IP) sample buffer (10 % β-mercaptoethanol, 2 % sodium dodoecyl sulphate (SDS), 30 % glycerol, 0.025 % bromophenol blue). The protein-bound glutathione Sepharose 4B beads and, as control, input TNT® *in vitro* translated product (1 µl) were resolved by SDS-PAGE and electroblotted onto PVDF membrane. The membranes were screened by immunoblot analysis with *anti*-HA (3F10) (1 in 1000, 5 % skimmed milk, TBS) and *anti*-GST (1 in 1000, 5 % skimmed milk, TBS), followed by chemiluminescence detection.

For GST pull-down assays using mammalian extracts, HEK.293 cells, transiently transfected with pCMVTag2b:AAMP some 48 hr prior to experiment, were lysed in buffer B (10 mM Tris-Cl, pH7.5, 150

mM NaCl, 0.5 % Triton-X-100, 10 µg/ml aprotinin, 10 µg/ml leupeptin, 0.5 mM PMSF). Cellular debris was removed by centrifugation (14,000 rpm, 4 °C, 20 min) and lysates (500 µg /pull-down) were incubated for 2 hr at 4 °C with glutathione sepharose beads pre-loaded with 10 µg GST.TPα$^{312-343}$, GST.TPβ$^{312-407}$, or expressing other subdomains of TPα/TPβ as listed and, as control, GST. Beads were washed thrice in buffer B followed by three changes in PBS. Proteins were solubilised in IP sample buffer and resolved by SDS-PAGE and electroblotted onto PVDF membrane. The membranes were screened by immunoblot analysis with *anti*-FLAG horseradish peroxidise (HRP)-conjugate and *anti*-GST (1 in 1000, 5 % skimmed milk, TBS) antibodies, followed by chemiluminescence detection.

Reverse transcriptase-polymerase reaction (RT-PCR).

In order to determine the sequence of AAMP, total RNA was extracted from HEL 92.1.7 and EA.hy 926 cells using TRI reagent (Sigma) and was subject to RT-PCR using oligonucleotide primers corresponding to nucleotides 1-18 of NM_001087 (5') and nucleotides 347-366 of NM_001087 (3'). Briefly, total RNA (1.4 µg) was converted to first strand cDNA with mouse moloney leukaemia virus (MMLV) RT in the presence of random hexamers (100 pM) in a 25 µl reaction, containing 1 mM dNTPs, 40 U RNasin, 1 U MMLV RT, 50 mM Tris–HCl, pH 8.3, 75 mM KCl, 3 mM $MgCl_2$, 10 mM DTT. Thereafter, 3.5 µl of first strand cDNA was used as template in each PCR reaction in the presence of 10 mM Tris HCl, pH 8.3, 50 mM KCl, 2 mM $MgCl_2$ 0.2 mM dNTPs, 6.7 % glycerol, 1 µM sense primer, 1 µM antisense primer and 1 U Taq DNA polymerase. Amplified PCR products were purified (Qiagen PCR purification kit) and subject to DNA sequence- and bioinformatic- analyses.

Computational Sequence Analysis & Structure Predictions.

Computational analysis of AAMP was performed by online submission to the Pfam database, a database of protein families that includes multiple sequence alignments generated using hidden Markov models (http://pfam.sanger.ac.uk/; [54]). Structure prediction of the AAMP was generated by online submission to the iterative (I)-TASSER algorithm, a 3-dimensional protein structure prediction software which builds models based on multiple-threading consensus target-to-template alignments by LOMETS (Local Meta-Threading-Server) and iterative TASSER simulations (http://zhang.bioinformatics.ku.edu/I-TASSER; [55, 56]).

Immunoprecipitations.

HEK.TPα, HEK.TPβ, HEK.β-galactosidase (HEK.β-Gal), were transiently co-transfected with pADVA and either pCMVTag2B:AAMP^{WT}, pCMVTag2B:AAMP$^{\Delta 348}$, pCMVTag2B:AAMP$^{\Delta 298}$, or pCMVTag2B:AAMP$^{\Delta 165}$, where specified, using Effectene transfection agent. EA.hy926 cells, 1° h.CoASMCs or 1° HUVECs were plated onto 10 cm dishes to achieve > 80 % confluence. In all cases prior to immunoprecipiatation, cells were washed in the appropriate serum-free media and either incubated with vehicle or with 1 µM U46619 for the times indicated in the figure legends. Thereafter, cells were washed

with ice-cold PBS and harvested in co-immunoprecipitation buffer (50 mM HEPES, pH 7.5, 50 mM NaCl, 10 % glycerol, 0.5 % NP-40, 2 mM EDTA, 100 µM Na_3VO_4, 1 mM PMSF, 4 µg/ml leupeptin and 2.5 µg/ml aprotinin). Lysates were clarified by centrifugation at 13,000 x g for 10 min and an aliquot (40 µl; approx 40 µg) retained for analysis of expression in whole cell lysates. The remaining lysate was used for immunoprecipitation, using *anti*-HA (101R; 1:300), *anti*-AAMP or *anti*-α-actinin antibodies to precipitate HA-tagged TPα, TPβ or β-Gal, and endogenously expressed AAMP (1:1000) and α-actinin (1:1000), respectively, through overnight incubation at 4 °C with rotation. Thereafter, lysates were incubated for 1 hr with either 50 % slurry of protein G-sepharose (10 µl) or protein A-sepharose (AAMP co-IP; 40 µl), prior to washing. Immunoprecipitates were resolved by SDS-PAGE, on 10 % acrylamide gels, and subjected to successive immunoblotting with *anti*-Flag antibody and *anti*-HA (3F10; 1:500), *anti*-α-actinin (1:1000) or *anti*-AAMP (1:1000) antibodies, as indicated.

Immunofluorescence and confocal microscopy.

To examine the expression and co-localization of AAMP with TPα or TPβ, HEK.TPα or HEK.TPβ cells were grown on poly-L-lysine treated coverslips, in 6-well plates for at least 48 hr. Thereafter, cells were fixed using 3.7 % paraformaldehyde, 1 X PBS, pH 7.4, for 15 min at RT prior to washing cells three times with PBS. Cells were permeabilized by incubation with 0.2 % Triton X-100 in PBS for 10 min on ice, followed by washing with 1 X TBS. Nonspecific sites were blocked by incubating cells with 1 % BSA, 1 X TBS, pH 7.4 for 1 hr at RT. Cells were co-incubated with the anti-HA 101R primary antibody (1:1,000 in 1 % BSA) to label the HA-tagged TPα or TPβ and the anti-AAMP primary antibody (1:150 in 1 % BSA) to label the endogenous AAMP for 1 hr at RT. The antibody solution was removed and cells were washed twice with 1 X TBS followed by further incubation with 1 % BSA for 30 min. Cells were then incubated with Alexa Fluor® 594 goat anti-mouse IgG secondary antibody (1:4,000 in 1 % BSA) to detect the HA-tagged receptors and/or Alexa Fluor® 488 goat anti-rabbit IgG secondary antibody (1:4,000 in 1 % BSA) to detect the AAMP for 1 hr at RT.

To examine expression of AAMP by indirect immunofluorescence in EA.hy926 cells, 1° hCoASMCs and/or 1° HUVECs, cells were grown on poly-L-lysine pre-treated coverslips to achieve 60-70 % confluence prior to fixation in 3.7 % paraformaldehyde in PBS for 15 min at RT. After washing three times in PBS, cells to be permeabilized were incubated with 0.2 % Triton X-100 in PBS for 10 min on ice followed by washing in three times in TBS. Non-specific sites were blocked by incubating cells with Blocking Buffer (1 % BSA in TBS) prior to immunolabeling with *anti*-AAMP (1:1000 dilution in Blocking Buffer) for 1 hr at RT. Unbound antibody was then removed by washing twice in TBS followed by detection with the secondary AlexaFluor488 goat *anti*-rabbit antibody (1:2000, in 1 % BSA, TBS).

To monitor changes in AAMP localization and/or its co-localization with α-actinin as a function of U46619 stimulation, EA.hy926 cells, 1° hCoASMCs and/or 1° HUVECs, at 60-70 % confluence on poly-L-lysine pretreated coverslips, were serum-starved for 1 hr in growth media containing 0.1 % FBS, prior to incubation with 1 µM U46619 for 0 – 240 min, as indicated in the specific figure legends. Cells were immunolabelled with *anti*-AAMP and *anti*-α-actinin under permeabilizing conditions, followed by detection

with the secondary AlexaFluor488 goat *anti*-rabbit antibody (1:2000, in 1 % BSA, TBS) and AlexaFluor594 goat anti-mouse (1:4000, in 1 % BSA, TBS), respectively.

After washing, all slides were counterstained with DAPI (1 μg/ml, in H_2O) prior to mounting coverslips in DakoCytomation fluorescence mounting medium. Imaging was carried out at 63x magnification using the Zeiss Axioplan 2 microscope and Axioplan Version 4.4 imaging software or using Carl Zeiss Laser Scanning System LSM 510 and Zeiss LSM Imaging Software, as indicated. Data presented in the figures are representative images from at least three independent experiments ($n \geq 3$) from which at least 10 fields were viewed at x 63 magnification, where the horizontal bar represents 10 μm. For quantification of the co-localization of AAMP with TPα or TPβ, overlay of pixels in the red and green channels was analyzed using the Intensity Correlation Analysis plugin available with WCIF ImageJ (Version 1.37c), where quantification is presented as the Pearson's Correlation coefficient [57].

Subcellular Fractionation.

HEK.TPα, HEK.TPβ and EA.hy926 cells (approx 2 x 10^6 cells in 8 ml MEM, 10 % FBS) were plated on 10-cm dishes some 48 hr previously to achieve approximately 75 % confluence. Thereafter, cells were washed and incubated in serum-free MEM for 1 hr prior to treatment with 1 μM U46619 for 0, 10, 60 or 240 min. An aliquot of total protein was retained for SDS-PAGE analysis while the remaining sample was subject to subcellular fractionation, as previously described [58]. Briefly, cell pellets were resuspended in homogenisation buffer (25 mM Tris–Cl, pH 7.5, 0.25 M sucrose, 10 mM $MgCl_2$, 1 mM EDTA, 0.1 M PMSF) and homogenised on ice for 1 min (approximately 20 strokes) prior to centrifuging samples at 100,000 ×g for 60 min at 4 °C. The soluble, supernatant (S_{100} fraction) was retained for analysis and the pellet (P_{100} fraction) was first washed in MES-KOH buffer (10 mM MES-KOH, pH 6.0, 10 mM $MnCl_2$, 1 mM EDTA,10 mM indomethacin) prior to resuspension in 10 mM Tris–Cl, 1 mM EDTA, pH 8.0. The protein concentrations were determined by the Bradford assay. Aliquots of the Total, S_{100} and P_{100} protein fractions (50 μg per lane) were resolved by SDS-PAGE, on 12.5 % gels, and subject to immunoblotting with *anti*-AAMP antibody (1:1000) followed by chemiluminescence detection.

Rho activation assays.

Activated cellular Rho was determined by interaction with a purified glutathione-S-transferase:rhotekin Rho-binding domain (GST-RBD) fusion protein immobilised on Glutathione-Sepharose 4B resin as previously described [41, 59]. Preparation of the GST-RBD protein was carried out as previously reported [59]. Briefly, for the 'Rho-pull-down assay', HEK.TPα, HEK.TPβ or 1° hCoASMCs cells were plated some 48 hr previously in complete growth medium onto 10-cm dishes to achieve ~70 % confluence; cells were then serum starved for 5 hr or 20 hr (1° hCoASMCs cells) in growth media containing 0.1 % FBS before stimulation for 0–10 min with 1 μM U46619, or as control, vehicle (0.01 % ethanol), as indicated in the figure legends. Thereafter, cells were lysed in 800 μl Lysis Buffer (125 mM HEPES, pH 7.5, 750 mM NaCl, 5 mM EDTA, 5 % NP-40, 10 % glycerol, 50 mM $MgCl_2$, 10 μg/ml leupeptin and 10 μg/ml aprotinin). Aliquots (600 μl) were subjected to pull-down using Glutathione-Sepharose 4B beads preloaded with 30 μg

GST-RBD, essentially as previously described [59]. Following washing, precipitated GTP-bound RhoA was subjected to SDS-PAGE on 12.5 % acrylamide gels and immunoblotted with *anti*-RhoA monoclonal antibody (Sc-418), followed by chemiluminescence detection [38]. In parallel, to confirm equivalent RhoA protein expression in the cell lysates and uniform protein loading, aliquots of whole cell lysates (typically 10 µl, corresponding to 1.25 % of total cell lysate) were directly immunoblotted with the *anti*-RhoA antibody and/or with the *anti*-AAMP antibody. All images of RhoA expression/pull-down were captured using Adobe Photoshop (V6), where band width and intensity was quantified and represented as fold increases relative to basal levels. To account for biological variations in basal activation levels, experiments were normalised to within a comparable range based on measurements from more than 20 individual experiments for each cell type.

Disruption of AAMP expression by small interfering (si)RNA.

For *small interfering* (*si*) RNA experiments, 1° hCoASMCs were plated at ~2.5 x 10^5 cells /35- mm plate and some 24 hr prior to transfection such that cells reach ~50 % confluence. Thereafter, cells were transfected with 0.2 µM AAMP *si*RNA (5' - CCCUAUCCAUGUACUGAAAtt, corresponding to nucleotides 828 - 846 of NM_001087; $siRNA_{AAMP}$), or as a control with its scrambled sequence ($siRNA_{Control}$) or 0.2 µM Lamin A/C *si*RNA (5'-CUGGACUUCCAGAAGAACAtt) using PrimeFect transfection reagent (Lonza), as per manufacturer's instructions. To confirm the efficacy of the *si*RNAs to disrupt AAMP expression, 1° hCoASMCs were harvested following incubation at 0, 24, 48, and 72 hr cells and subject to SDS-PAGE (10 – 15 µg/lane on 10 % gels) followed by electroblotting onto PVDF membranes (Roche). Membranes were initially screened versus the *anti*-AAMP antibody and, following stripping, were rescreened versus *anti*-HDJ-2 antibody to confirm uniform protein loading.

Migration assays.

In order to monitor changes in 1° hCoASMC migration, cells were plated in 12-well plates such that they were ≥ 90 % confluent 24 - 36 hr post-seeding. Thereafter, cells were either transfected with *si*RNA ($siRNA_{AAMP}$ or $siRNA_{Control}$) as described above or pre-incubated in reduced serum media (1 % FBS) 12-16 hr prior to scoring the cells from top-to-bottom perpendicular to pre-drawn lines (2 parallel lines approx 3-4 mm) on the underside of the well using a 200 µl pipette tip. Loose cells and debris was washed away with serum-free media and replaced with reduced serum media (1 % FBS). Scratch wounds were imaged immediately or following incubation with 1 µM U46619, 20 ng/ml VEGF or, as control, vehicle, for the indicated times. All images were taken using a Nikon TMS inverted microscope with Matrox Intellicam software (version 2.07) and analysed with TScratch software (Version 1.0).

Data analyses.

Statistical analyses were carried out using the unpaired Student's t test throughout. *P*-values of less than or equal to 0.05 were considered to indicate a statistically significant difference.

Results & Discussion.

Identification of AAMP as an Interactant of TPα/TPβ in Yeast.

In order to identify novel proteins that may specifically interact with the human thromboxane (TX) A_2 receptor (TP), a yeast-2-hybrid (Y2H) screen of a human kidney cDNA library was performed using the carboxyl-terminal (C)-tail domains of TPα (TPα$^{312-343}$) and TPβ (TPβ$^{312-407}$), encoding sequences both common (residues 312-328) and unique (TPα, residues 329-343; TPβ, residues 329-407) to the individual receptor isoforms as specific bait proteins (**Figure 1A**). Following primary high-stringency and secondary screenings of the human kidney cDNA library (complexity 3.5 x 10^6 independent clones), positive clones from the TPβ screen were found to encode angio-associated migratory cell protein (AAMP), a WD-40 domain protein also showing sequence homology to the immunoglobulin (Ig) superfamily including certain cellular-adhesion proteins [1, 12, 60]. The clones identified encode the C-terminal 308-434 residues of AAMP encompassing its putative membrane association domain and 2 of its proposed WD-40 repeat motifs. The interaction with AAMP$^{308-434}$ was further examined by direct mating of the MATa *S.c* Y187 (pACT2:AAMP$^{308-434}$) prey strain with transformants of the MATα *S.c* AH109 (pGBKT7) bait strain encoding the entire or unique C-tail domains of TPα (residues 312-343 or 329-343, respectively) and TPβ (residues 312-407 or 329-407, respectively), where the unrelated bait p53 or the empty vector, pGBKT7, served as controls. While each of the bait and prey strains mated successfully, strains encoding TPα$^{312-343}$, TPα$^{329-343}$, p53 or pGBKT7 alone failed to show an interaction with AAMP$^{308-434}$ (**Figure 1B**). On the other hand, both TPβ$^{312-407}$ and TPβ$^{329-407}$ exhibited a strong interaction with AAMP$^{308-434}$ (**Figure 1B**). These data indicate that AAMP$^{308-434}$ interacts specifically with the C-tail domain of TPβ as assessed by Y2H-based screening.

To further analyse the interaction with AAMP, glutathione S-transferase (GST) pull-down assays were performed using purified GST-fusion proteins of TPα$^{312-343}$, TPα$^{329-343}$, TPβ$^{312-407}$, TPβ$^{329-407}$ and, as a control, GST alone versus an *in vitro* transcribed & translated form of AAMP$^{308-434}$ (**Figure 1C**). Consistent with studies in yeast, AAMP$^{308-434}$ showed strong interaction with both TPβ$^{312-407}$ and TPβ$^{329-407}$ but not with TPα$^{329-343}$ or GST alone. However, the data indicated a weak interaction between AAMP$^{308-434}$ with TPα$^{312-343}$ encoding the entire C-tail domain of TPα including that region (residues 312-328) also common to TPβ. Immunoblotting with *anti*-GST confirmed uniform protein loading of each purified recombinant protein in the pull-down assays although, in certain, cases some degradation was consistently observed (**Figure 1C**, lower panel).

AAMP interacts with both TPα and TPβ in Mammalian Cells.

Following initial cloning of its cDNA, the deduced primary sequence of AAMP was originally predicted to be a 452 aa WD-40 domain protein also containing a putative N-terminal heparin-binding (HB) motif (**Figure 2A**). However, a discrepancy exists in the literature between the deduced primary sequence of AAMP [1] and that sequence (NM_001087) deposited at the National Center for Biotechnology Information (NCBI) data base. The basis of this discrepancy relates to the identity of nucleotides 31-33 of the AAMP

primary (1^{o}) transcript, which were originally proposed to correspond to an 'AUG' codon and to represent the translational initiation codon immediately upstream of the HB coding sequence [1]. In contrast, in the deposited sequence (NM_001087), the first in-frame initiation codon is actually located at nucleotides 85-87 downstream of the putative HB coding sequence and thereby is predicted to encode a smaller protein of 434 residues. Hence, owing to this discrepancy and as the HB domain was originally proposed to be of possible functional relevance, it was deemed necessary to clarify the sequence of AAMP, in particular surrounding the translational initiation codon and HB domain. Therefore, RT-PCR followed by nucleotide sequence analysis of mRNA extracted from two independent cell lines, namely human erythroleukemic (HEL) 92.1.7 and the human vascular endothelial EA.hy926 cells was used to clarify the sequence of AAMP. Sequence analysis of a number of independent amplifications from both cell lines confirmed that nucleotides 31-33 do not correspond to an AUG initiation codon and that the first in-frame initiation codon is located at 85-87 (**Figure 2B**). Hence, it is concluded that AAMP is a 434 aa protein and does not contain the proposed HB domain.

Having clarified its sequence, the ability of the full-length AAMP (residues 1 -434, hereon in referred to as AAMP) expressed in lysates from transfected mammalian human embryonic kidney (HEK) 293 cells to interact with GST.TPα$^{312\text{-}343}$, GST.TPβ$^{312\text{-}407}$ or, as controls, with GST was investigated through GST pull-down assays. AAMP specifically interacted with both GST.TPα$^{312\text{-}343}$ and GST.TPβ$^{312\text{-}407}$ but not with GST alone (**Figure 2C**). Furthermore, the ability of AAMP to interact with haemagglutinin (HA)-tagged forms of full length TPα or TPβ, stably expressed in the previously characterised HEK.TPα and HEK.TPβ cell lines [37], was investigated through co-immunoprecipitations. HEK.TPα, HEK.TPβ cells or, as controls, HEK.β-Gal cells, encoding HA-tagged β-galactosidase (β-Gal), were transfected with plasmid encoding AAMP and its presence in the *anti*-HA precipitates examined. AAMP was detected in the immunoprecipitates from both HEK.TPα and HEK.TPβ cells, but not from control HEK.β-Gal cells (**Figure 2D**, upper panel). Failure to detect AAMP in the latter immunoprecipitates was not due to its reduced expression (**Figure 2D**, lower panel) or due to failure of the immunoprecipitation in HEK.β-Gal cells *per se* (**Figure 2D**, middle panel). Taken together, these data confirm a specific interaction between AAMP with both TPα and TPβ isoforms.

As an additional means of examining the novel interaction, confocal image analysis was also used to investigate the expression and possible co-localization of TPα and TPβ with AAMP endogenously expressed in the HEK.TPα and HEK.TPβ clonal cell lines. Consistent with previous reports [61], while TPα is almost exclusively expressed at the plasma membrane, TPβ differs in that it is expressed both at the plasma membrane but also as an intracellular reserve associated with the endoplasmic reticulum (**Figure 2E**, *anti*-HA panels). Immunostaining of endogenous AAMP in the latter cell lines was examined using an affinity purified antibody directed to the C-terminal residues of AAMP (~ 334 – 434; Strategic Diagnostics Incorporated) and established that it is expressed both at the plasma membrane and in the cytosolic fraction where it displayed extensive punctate staining, possibly associated with a fibrous network (**Figure 2E**, *anti*-AAMP panels). Moreover, in the overlay panels, TPα and AAMP showed co-localization mainly at the

plasma membrane, while no co-localization was evident in the cytosolic fraction (**Figure 2E**, *Overlay,* upper panel). In contrast to this, TPβ and AAMP showed more extensive co-localization at the plasma membrane and, to a lesser extent, intracellularly while in certain other regions, it was clear that there was no co-localization between AAMP with TPβ (**Figure 2E**, *Overlay*, lower panel). Furthermore, use of the Pearson's correlation coefficient (Rr) for quantitation of the co-localisation with AAMP in the latter fluorescent images established that while both TP isoforms showed a positive co-localisation (Rr $\neq 0$, and between 0 and + 1), the extent of co-localisation of TPβ with AAMP (Rr = 0.352 ± 0.017) was substantially greater than that of TPα (Rr = 0.157 ± 0.042).

Identification of the regions within TPα and TPβ interacting with AAMP.

It was next sought to identify the specific regions within the C-tail domains of TPα and TPβ responsible for their interaction with AAMP through a series of deletion analyses in combination with Y2H-based screening and GST-pull down assays (**Figure 3A & 3B**, respectively). Consistent with previous Y2H data (Figure 1B), strains encoding TPα$^{312\text{-}343}$ and TPα$^{329\text{-}343}$or, the controls, p53 and vector alone (pGBKT7) failed to show an interaction with AAMP$^{308\text{-}434}$ (**Figure 3A**). On the other hand, TPβ$^{312\text{-}407}$, TPβ$^{312\text{-}392}$, TPβ$^{329\text{-}407}$ and TPβ$^{329\text{-}392}$ exhibited a strong interaction with AAMP$^{308\text{-}434}$ while TPβ$^{312\text{-}366}$ and TPβ$^{312\text{-}353}$ both showed weaker interactions. Conversely, the shorter TPβ$^{329\text{-}366}$ and TPβ$^{329\text{-}353}$ subfragments failed to interact with AAMP$^{308\text{-}434}$ (**Figure 3A**). Hence, these data suggest a role for residues 312-328, located within the common region of the C-tail domain of TPα/TPβ as important for the interaction of TPβ with AAMP$^{308\text{-}434}$ in addition to the region C-terminal of residues 353/366. In keeping with the latter, the fragment TPβ$^{353\text{-}407}$ was sufficient to mediate a strong interaction with AAMP$^{308\text{-}434}$ in yeast (**Figure 3A**).

Consistent with previous reports [1, 13], AAMP is abundantly expressed in cells derived from the vasculature including in platelets, 1° hCoASMCs, 1° h aortic (Ao) SMCs, 1° HUVECs and in the vascular endothelial EA.hy926 cell line (**Figure 3B**). Hence, owing to the abundant expression of AAMP in the endothelial EA.hy926 cell line [62], GST-pull-down assays were performed using GST-fusion proteins based on various subfragments derived from the C-tail domains of TPα, TPβ or GST alone where lysates prepared from EA.hy926 cells served as a convenient source of endogenously expressed AAMP (**Figure 3C**). Concurring with previous data from transfected HEK 293 cells (**Figure 2D**), AAMP was found to interact with GST.TPα$^{312\text{-}343}$ and GST.TPβ$^{312\text{-}407}$, corresponding to the entire C-tail domains of TPα and TPβ, respectively, but did not interact with GST alone (**Figure 3C**). In contrast, AAMP did not interact with GST:TPα$^{329\text{-}343}$, corresponding to the unique C-tail domain of TPα, thereby suggesting that residues 312-328 common to both TPα and TPβ is required for the interaction of TPα with full length AAMP endogenously expressed in mammalian cells. With respect to TPβ, AAMP showed comparable interaction with GST:TPβ$^{312\text{-}407}$ and its subfragment GST:TPβ$^{312\text{-}392}$ but somewhat reduced ability to interact with GST:TPβ$^{312\text{-}366}$ and GST:TPβ$^{312\text{-}353}$ (**Figure 3C**). Similarly, on deletion of the common region (residues 312-328) from the C-tail domain of TPβ, AAMP interacted with GST:TPβ$^{329\text{-}407}$ and GST:TPβ$^{329\text{-}392}$, and to comparable levels, but not with the GST:TPβ$^{329\text{-}366}$ or GST:TPβ$^{329\text{-}353}$ (**Figure 3C**). This is in accordance

with the Y2H data and confirms a role for the region C-terminal of residues 353/366 of TPβ in its interaction with AAMP. Furthermore, the data suggests that in the absence of residues 353/366-407, the region common region (residues 312-328) is sufficient to mediate the interaction of TPβ, albeit to a lesser extent (compare $TP\beta^{312-353}$/$TP\beta^{312-366}$ to $TP\beta^{329-353}$/$TP\beta^{329-366}$; **Figure 3C**). Furthermore, AAMP interacted with GST:$TP\beta^{353-407}$ and, to a lesser extent, GST:$TP\beta^{353-392}$ and GST:$TP\beta^{366-392}$ (data not shown) but not with GST:$TP\beta^{353-366}$ (**Figure 3C**). These latter data provide further evidence that the critical residues for the interaction of TPβ with AAMP lie between residues 366 - 392. Immunoblotting with *anti*-GST confirmed uniform protein loading of each purified recombinant protein in the pull-down assays although, as previous, some degradation was consistently observed in certain cases (**Figure 3C**, lower panels).

Collectively, data from Y2H screening, involving $AAMP^{308-434}$, and GST-pull-down assays with AAMP endogenously expressed in endothelial EA.hy926 cells identify two regions of importance for its interaction with the intracellular C-tail domain of TPβ; namely, the proximal common region (residues 312-328) and a more distal C-terminal region (residues 366-392) unique to TPβ **(Figure. 3A & 3C)**. Additionally, in terms of TPα, the presence of the common region (residues 312-328) was sufficient and required for its interaction with full-length AAMP endogenously expressed in EA.hy926 cells but was not sufficient to mediate the interaction of TPα with $AAMP^{308-434}$ as neither $TP\alpha^{312-343}$ nor $TP\alpha^{329-343}$showed an interaction in yeast. Noteworthy, attempts to express full length AAMP (residues 1-434) in the pACT2 prey vector in yeast were not successful and, hence, it was not possible to carry out Y2H screening of the TPα or TPβ subfragments using AAMP in that system. Moreover, the possible involvement of the 3 intracellular (IC) loops, namely IC_1 (residues 52-70), IC_2 (residues 129-149) and IC_3 (residues 221-246) in the interaction with AAMP was also investigated using GST-pull-down assays (**Figure 3C**) and Y2H matings (data not shown). As depicted in **Figure 3C**, neither IC_1, IC_2 nor IC_3, expressed as GST-fusion proteins, interacted with AAMP. However, owing to the limited sizes of those sub-domains, the results generated may be inconclusive and, therefore, the possibility that any one of all of the IC domains may contribute to the interaction between TPα/TPβ with AAMP in mammalian cells cannot be excluded.

Identification of the regions of AAMP interacting with TPα and TPβ.

AAMP was originally predicted to contain 6 repeat WD-40 domains, a putative membrane-association domain and 2 Ig-homology domains (**Figure 4A**;[1]). In agreement with this, computational structural analysis of AAMP using the iterative TASSER (I-TASSER) algorithm [55, 56] also predicts that it contains 6 major WD-40 repeats of anti-parallel β-sheets structurally arranged in a manner reminiscent of the β-propeller structures of other WD-40-repeat containing proteins, such as the G-protein β subunit [8, 9], in addition to containing a disorganized linker region located between WD-40 domains 4 and 5 which maps to the proposed membrane association domain of AAMP (**Figure 4A & 4B**).

Hence, having mapped the major regions within the C-tail domains of TPα and TPβ involved in their interaction with AAMP, it was sought to identify the regions/subdomains within AAMP itself involved. To this end, FLAG-epitope tagged forms of either full length AAMP or 3 sub-deletions, namely $AAMP^{\Delta 348}$,

$AAMP^{\Delta 298}$ and $AAMP^{\Delta 165}$ (**Figure 4A**) were expressed in HEK.TPα, HEK.TPβ and, as controls, HEK.β-Gal cells and their ability to interact with HA-tagged TPα, TPβ, or β-Gal investigated through co-immunoprecipitation studies (**Figure 4C**). Consistent with previous data (**Figure 2D**), abundant FLAG-tagged AAMP was detected in immunoprecipitates from HEK.TPα and HEK.TPβ cells but not from HEK.β-Gal cells ($AAMP^{WT}$, **Figure 4C, upper panel**). Furthermore, each of the truncated AAMP proteins was detected in the TPα and TPβ immunoprecipitates, but not from HEK.β-gal cells, and at levels comparable to that of $AAMP^{WT}$ with the exception of $AAMP^{\Delta 165}$, containing WD-40 domains 1 & 2 only, which showed a weaker but specific interaction with both TP isoforms (**Figure 4C, upper panel**). Any observed differences in immunoprecipitation of AAMP, or of its subfragments, were not due to differences in their expression levels in the HEK.TPα, HEK.TPβ or HEK.β-gal cell lines or in the efficiency of the immunoprecipitations *per se* (**Figure 4C; lower and middle panels, respectively**). Hence, collectively, these data further confirm a physical interaction between TPα/TPβ and AAMP in mammalian cells that does not require a particular domain or defined region within AAMP but suggests that multiple sites throughout the protein may be involved.

Agonist-stimulation of TP disrupts the interaction with AAMP.

To further examine the interaction with AAMP, it was sought to investigate the effect of agonist-activation of TPα and TPβ on that interaction, initially in HEK.TPα and HEK.TPβ cells. Stimulation with the TXA_2 mimetic U46619 over a 0 – 24 hr period did not affect the overall level of endogenous AAMP expression in either clonal cell line (**Figure 5A**). Thereafter, the effect of U46619 on the interaction with AAMP was examined in HEK.TPα and HEK.TPβ cells through co-immunoprecipitations. In agreement with previous immunoprecipitations (**Figure 2D & 4C**), in the absence of agonist AAMP was detected in the *anti*-HA immunoprecipitates from both HEK.TPα and HEK.TPβ cells but was not associated with the immune-complexes from control HEK.β-Gal cells (**Figure 5B**). Following 10 min stimulation with U46619, there was a significant decrease in the level of AAMP in the immunoprecipitates from both cell types (**Figure 5B, upper panels** & **Figure 5C**; $p = 0.0008$ and $p = 0.0013$, respectively) while at 2 hr post-agonist stimulation the level of AAMP in the immunoprecipitates returned to those levels observed in the absence of agonist-stimulation (**Figure 5B, upper panels & Figure 5C**). Differences in levels of AAMP associated with the immune-complexes were not due to differences in the overall level of AAMP or in the efficiency of the immunoprecipitations *per se* (**Figure 5B, lower & middle panels, respectively**). Collectively, these data confirm that AAMP interacts constitutively with both TPα and TPβ but that in response to agonist-activation, there is a rapid and transient dissociation of AAMP from the receptor complex.

AAMP expression has been previously examined through cellular fractionation in human arterial smooth muscle cells where it was found to be predominantly expressed in the membranous fraction but was also present in the cytosolic fraction with no evidence of nuclear expression [13]. Herein, the effect of U46619 stimulation on the subcellular expression of AAMP endogenously expressed in HEK.TPα, HEK.TPβ and EA.hy926 cells was examined using, as previous (**Figure 2E**), the antibody directed to the C-

terminal region of AAMP (Strategic Diagnostics Incorporated). Consistent with previous reports [13], in the absence of agonist AAMP was abundantly expressed in the membrane (P_{100}) fraction with slightly reduced levels in the soluble (S_{100}) fraction (**Figure 6A**). Moreover, there were no measurable changes in AAMP expression in either the S_{100} or P_{100} fractions following short term (10 min) or more prolonged (1 – 4 hr) stimulation with U46619 (**Figure 6A**). Likewise, and in agreement with previous data (**Figure 5A**), U46619 did not mediate overall changes in total AAMP expression in any of the cell lines examined (**Figure 6A, lower panels**).

The effect of agonist-activation on the subcellular localization of AAMP endogenously expressed in 1^{o} CoASMCs and the endothelial EA.hy926 cell line was also investigated by indirect immunofluorescence microscopy. It was originally proposed that AAMP may display both intracellular (membrane and cytosolic) and extracellular membrane association, largely due to the presence of its membrane association domain [2]. However, more recent reports found no biophysical evidence for a transmembrane domain or secreted forms of AAMP in cultured rat smooth muscle cells [13]. In agreement with the latter, immunofluorescence staining of 1^{o} CoASMCs (**Figure 6B**) and EA.hy926 cells (data not shown) under permeabilizing, but not under non-permeabilizing, conditions showed abundant cytosolic and membrane expression where it exhibited a fibrous network appearance.

Thereafter, the effect of U46619 stimulation on the expression of AAMP was examined in the 1^{o} CoASMCs (data not shown) and EA.hy926 cells (**Figure 6C**) where cells were processed for imaging under permeabilizing conditions. Similar to that observed in HEK.TPα, HEK.TPβ cells and 1° hCoASMCs (**Figure 2E & 6B**), in the absence of agonist, AAMP showed extensive cytoplasmic and membrane expression, being largely associated with the plasma membrane and with a network of intracellular fibres extending to the cell periphery (**Figure 6C, Vehicle**). On agonist stimulation, there was a transient relocalization of AAMP whereby at 10 min post-U46619 stimulation, its association with the fibrous network dissipated and exhibited more punctate staining within the cytosol (**Figure 6C, U46619, 10 min**) while at 30 min and more prolonged (1 – 4 hr) post-agonist stimulation there was a reappearance of its association with the fibrous network (**Figure 6C, U46619**). Hence, taken together, these data establish that while there is no alteration in the overall level or subcellular distribution of AAMP between the membrane (P_{100}) and cytosolic (S_{100}) fractions in response to agonist-activation, there is a transient dissociation of AAMP from the TPα/TPβ complex that coincides with its relocalization from more organized fibrous network to a more punctate appearance within the cell.

Association between AAMP and TP does not influence their ability to regulate RhoA.

TXA_2 is a potent mediator of F-actin polymerization and smooth muscle contraction that can occur through its ability to regulate both the Ca^{2+} dependent- and RhoA/Ca^{2+} independent mechanisms [63]. Moreover, while both TPα or TPβ show similar activation of G_{12}/RhoA, their responses are subject to independent, differential feedback regulation by the vasodilatory autocoids prostacyclin and nitric oxide [41]. In addition, over-expression of AAMP in human smooth muscle led to increased association of RhoA with membrane

fractions suggesting that AAMP may influence RhoA activation status [13]. Hence, as RhoA appears to be a common downstream effector of the TPs and of AAMP, the possible influence of ectopic expression of AAMP on U46619-mediated RhoA activation was investigated in 1^{o} CoASMCs and in HEK.TPα and HEK.TPβ cells using the 'Rho pull-down assay' based on its effector Rhotekin [59].

In the absence of agonist, low to moderate levels of active Rho were detected in lysates obtained from HEK.TPα, HEK.TPβ and 1° hCoASMCs (Active Rho, **Figure 7A**). Consistent with previous reports [41], both TPα and TPβ mediated substantial increases (approx. 20-fold) in RhoA activation in HEK.TPα and HEK.TPβ cells in response to U46619 stimulation, with a smaller increase (5-fold) observed in 1° hCoASMCs (Vector; **Figure 7A & 7B**). Over-expression of AAMP in non-stimulated HEK.TPα and HEK.TPβ cells resulted in 2 – 4 fold increases in active Rho levels compared to control cells transfected with the empty vector alone (**Figure 7**). Likewise, in 1° hCoASMCs cells over-expression of AAMP resulted in an increase, albeit small (approx. 10 % increase compared to vector control), in Rho activity in the absence of agonist. However, there were no measurable agonist-dependent increases in RhoA activity in either cell type following transient over-expressing of AAMP (**Figure 7A & 7B**). Any observed differences in RhoA activity in the various assays were not due to changes in the levels of Rho present in the whole cell lysates *per se* (**Figure 7A;** Total Rho) while screening with the *anti*-AAMP antibody confirmed near equivalent level of endogenous and over-expressed AAMP in the different assays (**Figure 7A;** *anti*-AAMP)

Collectively, these data confirm substantial agonist-induced activation of RhoA by both TPα and TPβ and suggest that while over-expression of AAMP leads to modest increases in RhoA activation in non-stimulated cells, it does not further enhance RhoA activation in response to U46619 stimulation. Hence, expression of AAMP does not appear to substantially affect RhoA signalling by the TPs.

***AAMP does not associate with α-actinin*.**

As stated, both TPα and TPβ mediate F-actin polymerization and smooth muscle contraction that occurs in part through its transient, time dependent activation of RhoA [41]. It has recently been proposed that AAMP may bind to the actin cross-linking protein α-actinin to regulate smooth muscle cell migration through a Rho-dependent mechanism [13, 64]. Therefore it was sought to investigate that hypothesis and, in view of the finding herein of a direct interaction between AAMP and the TPα/TPβ isoforms, to query whether the proposed association between AAMP and α-actinin might be affected in response to TP activation.

To investigate whether AAMP may form a complex, be it direct or indirect, with α-actinin, EA.hy926 cells were incubated with U46619 (0 – 4 hr) prior to immunoprecipitation of endogenous AAMP with *anti*-AAMP (**Figure 8A**) or endogenous α-actinin with *anti*- α-actinin (**Figure 8B**) and subsequent screening of immune-complexes with *anti*-α-actinin and *anti*-AAMP antibodies, respectively (**Figure 8A & 8B**). In the absence of agonist, α-actinin was not detected in the *anti*-AAMP immunoprecipitates (**Figure 8A, upper panel**). Moreover, stimulation of EA.hy 926 cells with U46619 (1 μM; up to 4 hr) did not promote an association of α-actinin with AAMP as evidenced by the failure to detect α-actinin in the *anti*-AAMP immunoprecipitates from U46619-treated cells (**Figure 8A, upper panel**). To confirm that lack of

interaction is not due to the inability of the *anti*-AAMP to immunoprecipitate, the converse immunoprecipitation was also performed and AAMP was not found in the *anti*-α-actinin immune-complexes regardless of the absence or presence of U46619 (**Figure 8B, upper panel**). Failure to detect α-actinin or AAMP in the immunoprecipitates was not due to lack of their expression in the cell lysates (**Figure 8A & 8B, 'Lys' & lower panels, respectively**).

To independently assess a possible association of AAMP with α-actinin, EA.hy 926 and 1° hCoASM cells were co-stained with *anti*-AAMP and *anti*-α-actinin antibodies under permeabilizing conditions followed by detection through image analyses with AlexaFluor488- and AlexaFluor594-labelled secondary antibodies, respectively. Consistent with previous imaging data (**Figure 6**), AAMP is predominantly localized to the cell periphery in both EA.hy926 and 1° hCoASM cells and also associates with a distinct intracellular fibrous network (**Figure 8C, EA.hy926 & 1° hCoASM cells, AAMP, Vehicle**). In response to U46619 stimulation, the intracellular fibrous network associated with AAMP dissipates in both cell types and adopts more punctate appearance after 10 min (**Figure 8C, AAMP, 10 min**) but reappears after 1 hr (data not shown) and more prolonged exposure to agonist (**Figure 8C, AAMP, 4 hr**). Both cell lines express abundant levels of α-actinin throughout the cytosol and extending to the cell membrane (**Figure 8C, α-Actinin, Vehicle**). Following U46619 stimulation, α-actinin becomes organised into or along *anti*-parallel fibers, reminiscent of actin microfilaments which, after prolonged exposure, become less organised and diffuse (**Figure 8C, α-actinin, 10 min & 4 hr**). The overlaid images in both cell types demonstrate that in the absence of agonist, there is no evidence of co-localization, except where their expression overlaps at the cell membrane (**Figure 8C, Overlay, Vehicle**). Following U46619 stimulation, there is no overall change in the overlapping expression at the cell membrane and despite changes in both AAMP and α-actinin, there is no evidence of an association between these 2 proteins (**Figure 8C, Overlay, 10 min & 4 hr**). Taken together, these data provide substantial evidence to suggest that AAMP does not associate or co-localize with the microfilament protein α-actinin and that such associations are not influenced by agonist activation of the TPs endogenously expressed in either 1° hCoASMCs or endothelial EA.hy926 cells.

AAMP small interfering RNA (siRNA) inhibits smooth muscle cell migration.

As its name suggests, AAMP has been linked to cell migration [1, 12, 13, 21, 60]. However, very little is known about the mechanism involved. Inhibition of AAMP through inhibitory recombinant-antibody treatment or *small interfering* RNA (*si*RNA)-mediated down-regulation was shown to reduce migration of SMCs while over-expression led to an increase in the migratory potential [13]. Herein, in view of the interaction between the TP isoforms and AAMP, the effect of *si*RNA-mediated knockdown of AAMP on the migration of 1° hCoASMCs was examined and in the absence and presence of U46619 stimulation.

Successful disruption of AAMP was confirmed in 1° hCoASMCs whereby transient transfection of *si*RNA based on AAMP specific sequences (NM_001087; nucleotides 828 – 846; $siRNA_{AAMP}$), but not the scrambled control sequence ($siRNA_{Control}$), resulted in near complete knockdown of AAMP expression at 24 hr post-transfection (**Figure 9A**). Furthermore, down-regulation of AAMP expression was maintained up to 72 hr post-transfection (**Figure 9A**, *anti*-AAMP). The decrease in AAMP expression was not due to unequal

loading of the protein samples as evidenced by immunoblotting of membranes for the ubiquitously expressed molecular chaperone HDJ-2/DNA-J protein, which served as an internal loading control (**Figure 9B**, *anti*-HDJ-2). Thereafter, 1° hCoASMCs were transfected with the *si*RNA$_{Control}$ or *si*RNA$_{AAMP}$ and cell migration assays performed 24 hr post-transfection using the wound-repair assay where cells were treated with U46619 or, as positive and negative controls, with VEGF or drug-vehicle, respectively. Scratch-wounds were created in 1° hCoASMC monolayers and imaged immediately (0 hr) or at 12 hr and 24 hr post-wound where TScratch software analysis programme was employed to quantify gap closure (**Figure 9C, Vehicle & U46619, respectively**). In the absence of stimulation, 1° hCoASMCs transfected with the *si*RNA$_{Control}$ migrated into the scratch wound and ~ 80 % closure was obtained after 24 hr (**Figure 9C, Vehicle, *si*RNA$_{Control}$, 24 hr**). Down-regulation of AAMP through *si*RNA$_{AAMP}$ slightly impaired that migration as evidenced by the reduced closure at 12 hr and 24 hr (**Figure 9C, Vehicle, *si*RNA$_{AAMP}$; $p = 0.21$ & $p = 0.0013$, respectively**). Consistent with numerous studies, VEGF enhanced 1°hCoASMC migration at 12 hr and 24 hr compared to vehicle treated cells (**Figure 9C, VEGF, *si*RNA$_{Control}$; 12 hr, $p = 0.099$, 24 hr, $p = 0.018$**). However, AAMP down-regulation did not affect VEGF-induced migration (**Figure 9C, VEGF, *si*RNA$_{AAMP}$; 12 hr, $p = 0.96$, 24 hr, $p = 0.82$**). In the presence of U46619, there was a modest reduction in migration of 1° hCoASMCs transfected with the *si*RNA$_{Control}$ compared to that of the vehicle-treated cells at 12 hr and 24 hr post-wound (**Figure 9C, U46619, *si*RNA$_{Control}$; 12 hr, $p = 0.12$, 24 hr, $p = 0.017$**). Furthermore, in the presence of U46619, migration of 1° hCoASMCs in *si*RNA$_{AAMP}$-transfected cells was delayed relative to that in cells transfected with *si*RNA$_{Control}$ such that in the presence of U46619 and *si*RNA$_{AAMP}$, the level of closure following 24 hr was significantly reduced from ~ 60% closure to less than 40% (**Figure 9C**, **U46619, *si*RNA$_{AAMP}$; 12 hr, $p = 0.029$, 24 hr, $p = 0.022$**). Hence, these data indicate that AAMP is important for efficient 1^{o} hCoASMC migration whereby its down-regulation impairs or delays wound repair. Furthermore, the data shows that despite its ability to induce RhoA activation, U46619 does not augment but rather leads to a slight inhibition of 1^{o} hCoASMC migration which is further diminished where levels of AAMP are reduced, such as in the presence of *si*RNA$_{AAMP}$. In contrast to this, VEGF significantly enhances migration of 1^{o} hCoASMCs, an effect which is not affected by AAMP down-regulation. Collectively, the data suggests that AAMP may overcome TP-mediated inhibition of 1^{o} hCoASMC migration and that AAMP-mediated and VEGF-mediated migration of 1^{o} hCoASMCs occur through independent mechanisms.

Taken together, this study has identified AAMP as a novel interacting partner of TPα and TPβ. Through yeast mating and GST-pull-down assays, it was confirmed that AAMP interacts directly with both receptor isoforms within the common C-tail sub-domain (residues 312 - 328) and also with residues 366 – 392 within the unique C-tail region of TPβ. Moreover, this interaction was confirmed in mammalian cells and was found to be constitutive. While agonist-activation of TP signalling did not affect AAMP expression or subcellular localization *per se*, it did lead to a transient dissociation of the TP/AAMP complex, such as from immune complexes, that coincided with a transient dissipation of AAMP from a fibrous network to a more punctate intracellular distribution. Both TP signalling and AAMP over-expression have been implicated in RhoA activation, contributing to smooth muscle contraction and/or migration, respectively [13,

41, 64]. However, herein it was determined that AAMP is a weak activator of RhoA and does not influence TP-mediated RhoA activation but, rather, it occurs independently. Consistent with previous reports [13], down-regulation of AAMP reduced SMC migration, an effect that was further enhanced in the presence of U46619 while VEGF-mediated migration was not affected. Taken together, as outlined in the model presented in **Figure 10**, the data herein provides possible new insights into role of TXA_2 and AAMP in cell migration of 1^o hCoASMCs whereby it is proposed that agonist-activation of the TPα/TPβ isoforms leads to RhoA activation and associated F-actin polymerization and cell rounding, but not to cell migration *per se*. Coincident with agonist-activation of the TPs, there is a transient dissociation of AAMP from the inactive TPα/TPβ-immune complexes allowing for/facilitating AAMP-induced cell migration, possibly mediated in part through its ability to regulate RhoA or through, as yet, other undefined mechanism(s) (**Figure 10A & 10B**). Disruption of AAMP expression through *si*RNA_{AAMP} led to a decrease in 1^o hCoASMC migration in the presence of U46619 and, to a lesser extent, in vehicle-treated cells but not in presence of VEGF (**Figure 10C**). Collectively, it is proposed that in the absence of agonist, AAMP appears to be recruited into an inactive complex with either TPα, TPβ or both. In response to U46619-activation, there is transient dissociation of the complex leading to TPα/TPβ -mediated RhoA activation and AAMP-mediated migration. Hence, it is proposed that TP-mediated RhoA activation alone is not sufficient to mediate 1^o hCoASMC migration but rather any migration that occurs in the presence of TXA_2 or its mimetic U46619 appears to be mediated, at least in part, by AAMP liberated from the inactive complex in response to TP-activation. Hence, there appears to be an agonist-dependent switch regulating the association of AAMP with the TPα/TPβ complex and AAMP-induced migration.

While certain aspects of this proposed model have yet to be fully validated, the involvement of AAMP in SMC migration might help to explain much of the somewhat conflicting data that exists in the literature regarding the role of TXA_2 in regulating SMC and/or endothelial cell migration. More specifically, despite its robust ability to promote RhoA activation and downstream signalling [16, 19, 41, 63, 65], several studies have indicated that TXA_2, or its mimetics, may inhibit cell migration [66-71] while a limited number of other studies suggest that it may be stimulatory [72-74]. Given the critical role of TXA_2 within the vasculature and bearing in mind the increasing recognition of the role of AAMP in neointima formation associated with atherosclerotic lesions or restenosis following vascular intervention [13, 64], the identification of a direct interaction between TPα and TPβ with AAMP is likely to be highly significant regarding the understanding of the molecular network of events that precedes such lesions and may also provide targets for therapeutic intervention. Disruption of AAMP expression, such as through *si*RNA-mediated or other small molecule approaches may offer an attractive therapeutic option to impair smooth muscle migration, such as in atherosclerotic lesions or restenosis in response to vessel injury, typified by a prothrombotic milieu where TXA_2 levels are likely to be elevated. However, greater delineation of the pathways downstream of AAMP is necessary to obtain a more in-depth understanding of the functional implications of the direct interaction between it and the TP isoforms in these processes.

Acknowledgements

We are grateful to Dr Marie Beckner, Pittsburg University Medical Center, Pennsylvania for the gift of pGEX-1λT:Angio-associated migratory cell protein. This work was supported by grants to BTK from the Science Foundation of Ireland (Grant No. SFI: 05/IN.1/B19) and the Health Research Board (Grant No. RP/2008/33).

References

[1] Beckner ME, Krutzsch HC, Stracke ML, Williams ST, Gallardo JA, Liotta LA. Cancer Res 1995;55(10):2140-2149.
[2] Beckner ME, Peterson VA, Moul DE. Microvasc Res 1999;57(3):347-352.
[3] Allander SV, Nupponen NN, Ringner M, Hostetter G, Maher GW, Goldberger N, Chen Y, Carpten J, Elkahloun AG, Meltzer PS. Cancer Res 2001;61(24):8624-8628.
[4] Adeyinka A, Emberley E, Niu Y, Snell L, Murphy LC, Sowter H, Wykoff CC, Harris AL, Watson PH. Clin Cancer Res 2002;8(12):3788-3795.
[5] Bielig H, Zurek B, Kutsch A, Menning M, Philpott DJ, Sansonetti PJ, Kufer TA. Mol Immunol 2009;46(13):2647-2654.
[6] Yu L, Gaitatzes C, Neer E, Smith TF. Protein Sci 2000;9(12):2470-2476.
[7] Neer EJ, Schmidt CJ, Nambudripad R, Smith TF. Nature 1994;371(6495):297-300.
[8] Sondek J, Bohm A, Lambright DG, Hamm HE, Sigler PB. Nature 1996;379(6563):369-374.
[9] Wall MA, Coleman DE, Lee E, Iniguez-Lluhi JA, Posner BA, Gilman AG, Sprang SR. Cell 1995;83(6):1047-1058.
[10] Orlicky S, Tang X, Willems A, Tyers M, Sicheri F. Cell 2003;112(2):243-256.
[11] Li D, Roberts R. Cell Mol Life Sci 2001;58(14):2085-2097.
[12] Beckner ME, Liotta LA. Lab Invest 1996;75(1):97-107.
[13] Vogt F, Zernecke A, Beckner M, Krott N, Bosserhoff AK, Hoffmann R, Zandvoort MA, Jahnke T, Kelm M, Weber C, Blindt R. J Am Coll Cardiol 2008;52(4):302-311.
[14] Nobes CD, Hall A. J Cell Biol 1999;144(6):1235-1244.
[15] Kinsella BT. Biochem Soc Trans 2001;29(Pt 6):641-654.
[16] Klages B, Brandt U, Simon MI, Schultz G, Offermanns S. J Cell Biol 1999;144(4):745-754.
[17] Miggin SM, Kinsella BT. Biochim Biophys Acta 2001;1539(1-2):147-162.
[18] Miggin SM, Kinsella BT. Mol Pharmacol 2002;61(4):817-831.
[19] Moers A, Nieswandt B, Massberg S, Wettschureck N, Gruner S, Konrad I, Schulte V, Aktas B, Gratacap MP, Simon MI, Gawaz M, Offermanns S. Nat Med 2003;9(11):1418-1422.
[20] Kaneko Y, Nakayama T, Saito K, Morita A, Sato I, Maruyama A, Soma M, Takahashi T, Sato N. Hypertens Res 2006;29(9):665-671.
[21] Huang JS, Ramamurthy SK, Lin X, Le Breton GC. Cell Signal 2004;16(5):521-533.
[22] Dassesse T, de Leval X, de Leval L, Pirotte B, Castronovo V, Waltregny D. Eur Urol 2006;50(5):1021-1031; discussion 1031.
[23] Li X, Wei J, Tai HH. Arch Biochem Biophys 2007;467(1):20-30.
[24] Nie D, Guo Y, Yang D, Tang Y, Chen Y, Wang MT, Zacharek A, Qiao Y, Che M, Honn KV. Cancer Res 2008;68(1):115-121.
[25] Hirata M, Hayashi Y, Ushikubi F, Yokota Y, Kageyama R, Nakanishi S, Narumiya S. Nature 1991;349(6310):617-620.
[26] Nusing RM, Hirata M, Kakizuka A, Eki T, Ozawa K, Narumiya S. J Biol Chem 1993;268(33):25253-25259.
[27] Raychowdhury MK, Yukawa M, Collins LJ, McGrail SH, Kent KC, Ware JA. J Biol Chem 1994;269(30):19256-19261.
[28] Raychowdhury MK, Yukawa M, Collins LJ, McGrail SH, Kent KC, Ware JA. J Biol Chem 1995;270(12):7011.
[29] Coyle AT, Kinsella BT. FEBS J 2005;272(4):1036-1053.
[30] Coyle AT, Kinsella BT. Biochem Pharmacol 2006;71(9):1308-1323.
[31] Coyle AT, Miggin SM, Kinsella BT. Eur J Biochem 2002;269(16):4058-4073.
[32] Coyle AT, O'Keeffe MB, Kinsella BT. FEBS J 2005;272(18):4754-4773.
[33] Gannon AM, Kinsella BT. J Lipid Res 2008;49(12):2590-2604.
[34] Gannon AM, Kinsella BT. J Cell Mol Med 2009;13(11-12):4571-4586.
[35] Gannon AM, Turner EC, Reid HM, Kinsella BT. J Mol Biol 2009;394(1):29-45.
[36] Miggin SM, Kinsella BT. Biochim Biophys Acta 1998;1425(3):543-559.
[37] Reid HM, Kinsella BT. J Biol Chem 2003;278(51):51190-51202.
[38] Walsh MT, Foley JF, Kinsella BT. J Biol Chem 2000;275(27):20412-20423.
[39] Hirata T, Ushikubi F, Kakizuka A, Okuma M, Narumiya S. J Clin Invest 1996;97(4):949-956.
[40] Foley JF, Kelley LP, Kinsella BT. Biochem Pharmacol 2001;62(2):229-239.

[41] Wikstrom K, Kavanagh DJ, Reid HM, Kinsella BT. Cell Signal 2008;20(8):1497-1512.
[42] Kelley-Hickie LP, Kinsella BT. Biochim Biophys Acta 2006;1761(9):1114-1131.
[43] Kelley-Hickie LP, O'Keeffe MB, Reid HM, Kinsella BT. Biochim Biophys Acta 2007;1773(6):970-989.
[44] Bockaert J, Fagni L, Dumuis A, Marin P. Pharmacol Ther 2004;103(3):203-221.
[45] Bockaert J, Roussignol G, Becamel C, Gavarini S, Joubert L, Dumuis A, Fagni L, Marin P. Biochem Soc Trans 2004;32(Pt 5):851-855.
[46] Rey M, Vicente-Manzanares M, Viedma F, Yanez-Mo M, Urzainqui A, Barreiro O, Vazquez J, Sanchez-Madrid F. J Immunol 2002;169(10):5410-5414.
[47] Reid HM, Mulvaney EP, Turner EC, Kinsella BT. J Biol Chem 2010;285(24):18709-18726.
[48] Wikstrom K, Reid HM, Hill M, English KA, O'Keeffe MB, Kimbembe CC, Kinsella BT. Cell Signal 2008;20(12):2332-2346.
[49] Bockaert J, Marin P, Dumuis A, Fagni L. FEBS Lett 2003;546(1):65-72.
[50] Gorman CM, Gies D, McCray G, Huang M. Virology 1989;171(2):377-385.
[51] Hayes JS, Lawler OA, Walsh MT, Kinsella BT. J Biol Chem 1999;274(34):23707-23718.
[52] Miggin SM, Lawler OA, Kinsella BT. Eur J Biochem 2002;269(6):1714-1725.
[53] Suggs JE, Madden MC, Friedman M, Edgell CJ. Blood 1986;68(4):825-829.
[54] Finn RD, Mistry J, Tate J, Coggill P, Heger A, Pollington JE, Gavin OL, Gunasekaran P, Ceric G, Forslund K, Holm L, Sonnhammer EL, Eddy SR, Bateman A. Nucleic Acids Res 2010;38(Database issue):D211-222.
[55] Roy A, Kucukural A, Zhang Y. Nat Protoc 2010;5(4):725-738.
[56] Zhang Y. Proteins 2009;77 Suppl 9:100-113.
[57] Li Q, Lau A, Morris TJ, Guo L, Fordyce CB, Stanley EF. J Neurosci 2004;24(16):4070-4081.
[58] O'Keeffe MB, Reid HM, Kinsella BT. Biochim Biophys Acta 2008;1783(10):1914-1928.
[59] Ren XD, Schwartz MA. Methods Enzymol 2000;325:264-272.
[60] Beckner ME, Krutzsch HC, Klipstein S, Williams ST, Maguire JE, Doval M, Liotta LA. Exp Cell Res 1996;225(2):306-314.
[61] Valentin F, Field MC, Tippins JR. J Biol Chem 2004;279(9):8316-8324.
[62] Bouis D, Hospers GA, Meijer C, Molema G, Mulder NH. Angiogenesis 2001;4(2):91-102.
[63] Offermanns S, Laugwitz KL, Spicher K, Schultz G. Proc Natl Acad Sci U S A 1994;91(2):504-508.
[64] Holvoet P, Sinnaeve P. J Am Coll Cardiol 2008;52(4):312-314.
[65] Offermanns S. Circ Res 2006;99(12):1293-1304.
[66] Ashton AW, Cheng Y, Helisch A, Ware JA. Circ Res 2004;94(6):735-742.
[67] Ashton AW, Ware JA. Circ Res 2004;95(4):372-379.
[68] Ashton AW, Yokota R, John G, Zhao S, Suadicani SO, Spray DC, Ware JA. J Biol Chem 1999;274(50):35562-35570.
[69] Benndorf RA, Schwedhelm E, Gnann A, Taheri R, Kom G, Didie M, Steenpass A, Ergun S, Boger RH. Circ Res 2008;103(9):1037-1046.
[70] de Leval X, Dassesse T, Dogne JM, Waltregny D, Bellahcene A, Benoit V, Pirotte B, Castronovo V. J Pharmacol Exp Ther 2006;318(3):1057-1067.
[71] Gao Y, Yokota R, Tang S, Ashton AW, Ware JA. Circ Res 2000;87(9):739-745.
[72] Daniel TO, Liu H, Morrow JD, Crews BC, Marnett LJ. Cancer Res 1999;59(18):4574-4577.
[73] Ishizuka T, Matsumura K, Matsui T, Takase B, Kurita A. J Cardiovasc Pharmacol 2003;41(4):571-578.
[74] Nie D, Lamberti M, Zacharek A, Li L, Szekeres K, Tang K, Chen Y, Honn KV. Biochem Biophys Res Commun 2000;267(1):245-251.

FIGURES

Figure 1

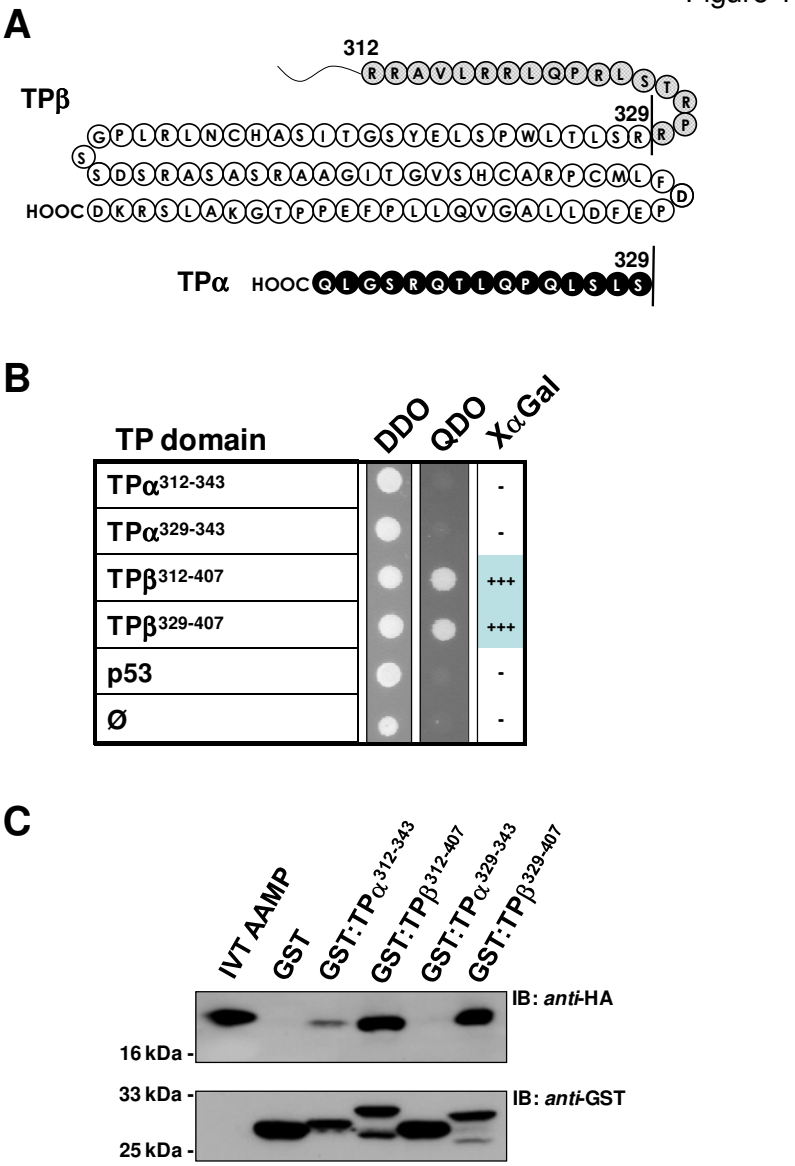

Figure 1. Interaction of AAMP with the carboxyl terminal (C)-tail domains of TPα and TPβ.
A. Schematic of the C-tail domains of TPα and TPβ, where residues 312 – 328 common to both isoforms are in grey, while residues unique to TPβ (aa 329-407) or TPα (aa 329-343) are in white and black, respectively. B. the *S.c* Y187 (pACT2:AAMP$^{308-434}$) prey strain was mated with *S.c* AH109 bait strains transformed with the indicated recombinant pGBKT7 plasmids or pGBKT7 alone (Ø). Diploids were selected on DDO media and interactants on QDO or on X-α-Gal media due to GAL4-dependent activation of the *ADE2* and *HIS3* or *MEL1* reporter genes due to interaction between the bait and prey proteins. C. *In vitro* pull-down assay of HA-tagged AAMP$^{308-434}$, produced by *in vitro* transcription and translation (IVT) of pACT2: AAMP$^{308-434}$, with Glutathione sepharose CL-4B beads preloaded with the indicated recombinant GST fusion proteins or, as a control, GST alone. Pull-down products or, as a control, an aliquot of the input IVT generated HA- AAMP$^{308-434}$ were resolved by SDS-PAGE and immunoblotted (IB) using *anti*-HA 3F10 or *anti*-GST antibody, followed by chemiluminescence detection. The relative positions of the molecular size markers (kDa) are indicated. Data; n ≥ 3.

Figure 2

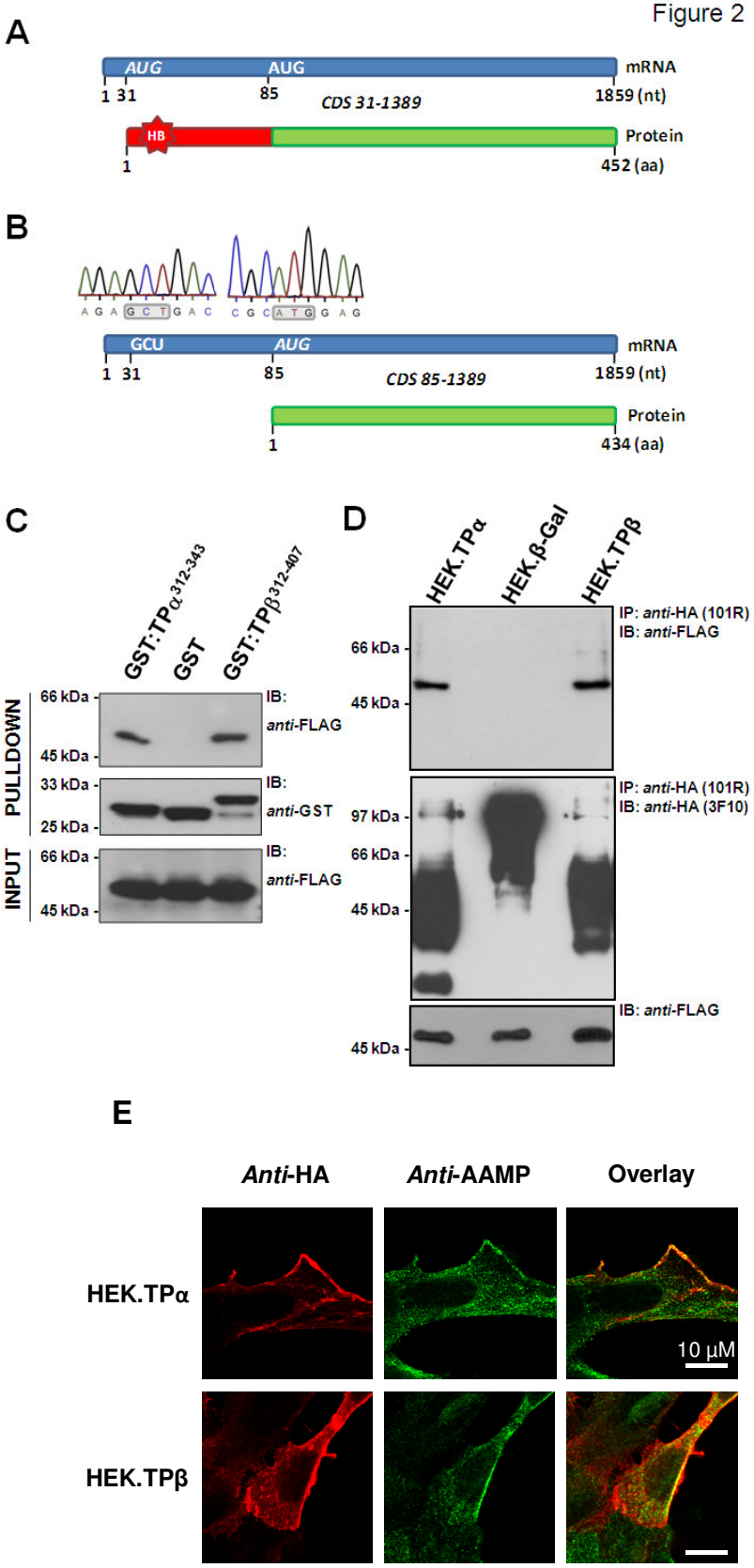
A
AUG
AUG
mRNA
1 31
85
CDS 31-1389
1859 (nt)
HB
Protein
1
452 (aa)
B
GCU
AUG
mRNA
1 31
85
CDS 85-1389
1859 (nt)
Protein
1
434 (aa)
C
GST:TPα 312-343
GST
GST:TPβ 312-407
PULLDOWN
66 kDa
45 kDa
IB: anti-FLAG
33 kDa
25 kDa
IB: anti-GST
INPUT
66 kDa
45 kDa
IB: anti-FLAG
D
HEK.TPα
HEK.β-Gal
HEK.TPβ
66 kDa
45 kDa
IP: anti-HA (101R)
IB: anti-FLAG
97 kDa
66 kDa
45 kDa
IP: anti-HA (101R)
IB: anti-HA (3F10)
45 kDa
IB: anti-FLAG
E
Anti-HA
Anti-AAMP
Overlay
HEK.TPα
HEK.TPβ
10 μM

Figure 2. Interaction of full-length AAMP with the TPα and TPβ in mammalian cells.
A. Schematic of the mRNA and deduced protein sequences of AAMP. Based on the proposal that an AUG initiation codon is located at nucleotide 31 in its 1^{o} transcript, AAMP is thought to have 452 residues with a heparin binding (HB) motif near its N-terminus. B. Sequence analysis of the AAMP cDNA from HEL 92.1.6 and EA.hy926 (data not shown) cells confirmed that the putative AUG codon at 31 is incorrect and that the first in-frame AUG initiation codon is at nucleotide 85. Hence, AAMP has 434 residues and does not have a HB motif. C. GST Pull-down assays using lysates from HEK 293 cells (500 µg/assay) transfected with pCMVTag2B:AAMP encoding FLAG-tagged full length AAMP versus the indicated GST protein. Pull-down products were resolved by SDS-PAGE and screened by immunoblotting (IB) using *anti*-FLAG (Upper panel) and *anti*-GST (Middle panel) antibody. D. HEK.TPα, HEK.TPβ and, as controls, HEK.β-Gal cells were transiently co-transfected with pCMVTag2B:AAMP prior to immunoprecipitation with *anti*-HA 101R antibody. Immunoprecipitates (IP) were resolved by SDS-PAGE and immunoblotted (IB) versus *anti*-FLAG (Upper panel) or *anti*-HA 3F10-HRP conjugated (Middle panel) antibody. To verify expression of the input AAMP proteins in Panels C & D, aliquots of whole cell lysates (~ 50 µg/lane) were immunoblotted with *anti*-FLAG antibody (Lower panels). The relative positions of the molecular size markers (kDa) are indicated to the left of the Panels C & D. E. HEK.TPα and HEK.TPβ cells were immuno-labelled with *anti*-HA and *anti*-AAMP antibodies under permeabilizing conditions followed by detection with *anti*-mouse AlexaFluor594 (*anti*-HA) and *anti*-rabbit AlexaFluor488 (*anti*-AAMP) conjugated secondary antibodies, respectively, or both (Overlay). Horizontal bar represents 10 µm. Data; $n \geq 3$.

Figure 3

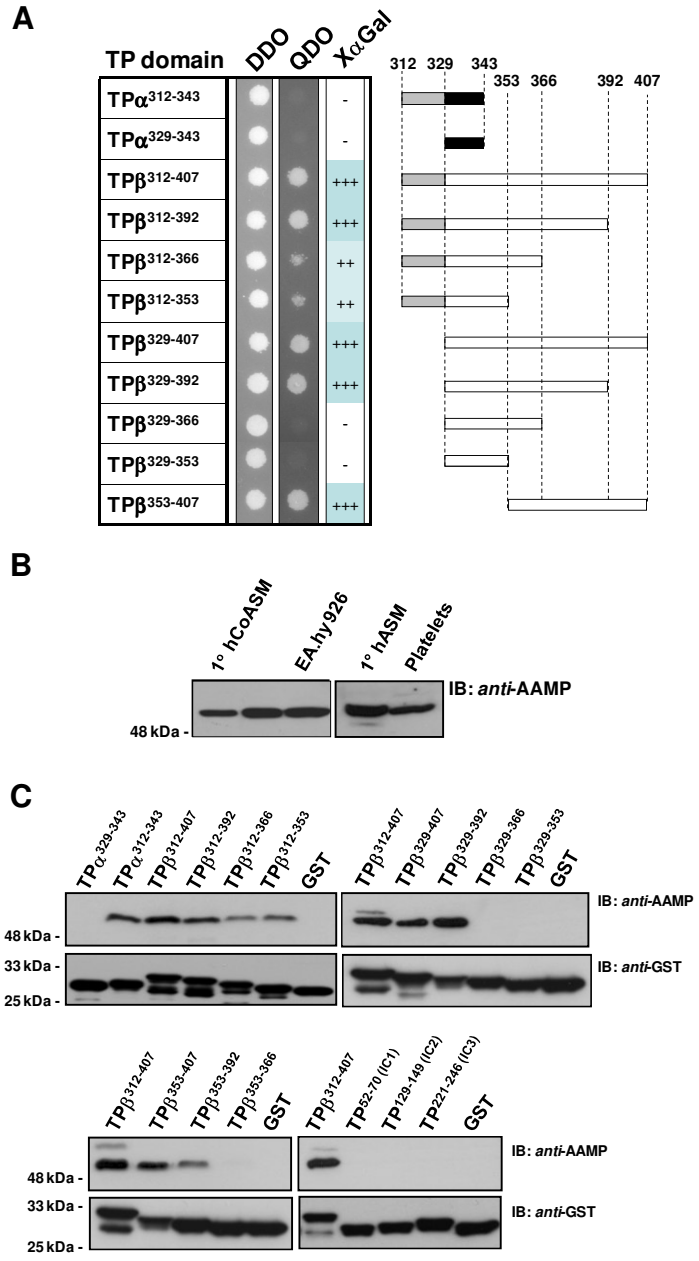

Figure 3: Identification of the regions with in TPα & TPβ mediating the interaction with AAMP.
A. The *S.c* Y187 (pACT2:AAMP$^{308-434}$) prey strain was mated with recombinant *S.c* AH109 (pGBKT7) bait strains encoding common or unique subfragments of the C-tail domains of TPα or TPβ, as listed. Diploids were selected on DDO media while interactants were selected on QDO and by their ability to cleave X- α-Gal. B. Western blot analysis of AAMP endogenously expressed in the indicated cell types (~ 50 µg/lane or corresponding to 2 X 10^8 washed platelets). C. *In vitro* pull-down assays of AAMP endogenously expressed in cell lysates (500 µg/assay) from EA.hy926 cells versus the indicated GST fusion proteins, where GST:TPβ$^{312-407}$ and GST alone served as positive and negative controls, respectively, in all cases. Pull-down products were resolved by SDS-PAGE and screened by immunoblotting (IB) using *anti*-AAMP (Upper panels) and *anti*-GST (Lower panels) antibody. The relative positions of the molecular size markers (kDa) are indicated. Data; n ≥ 3.

Figure 4

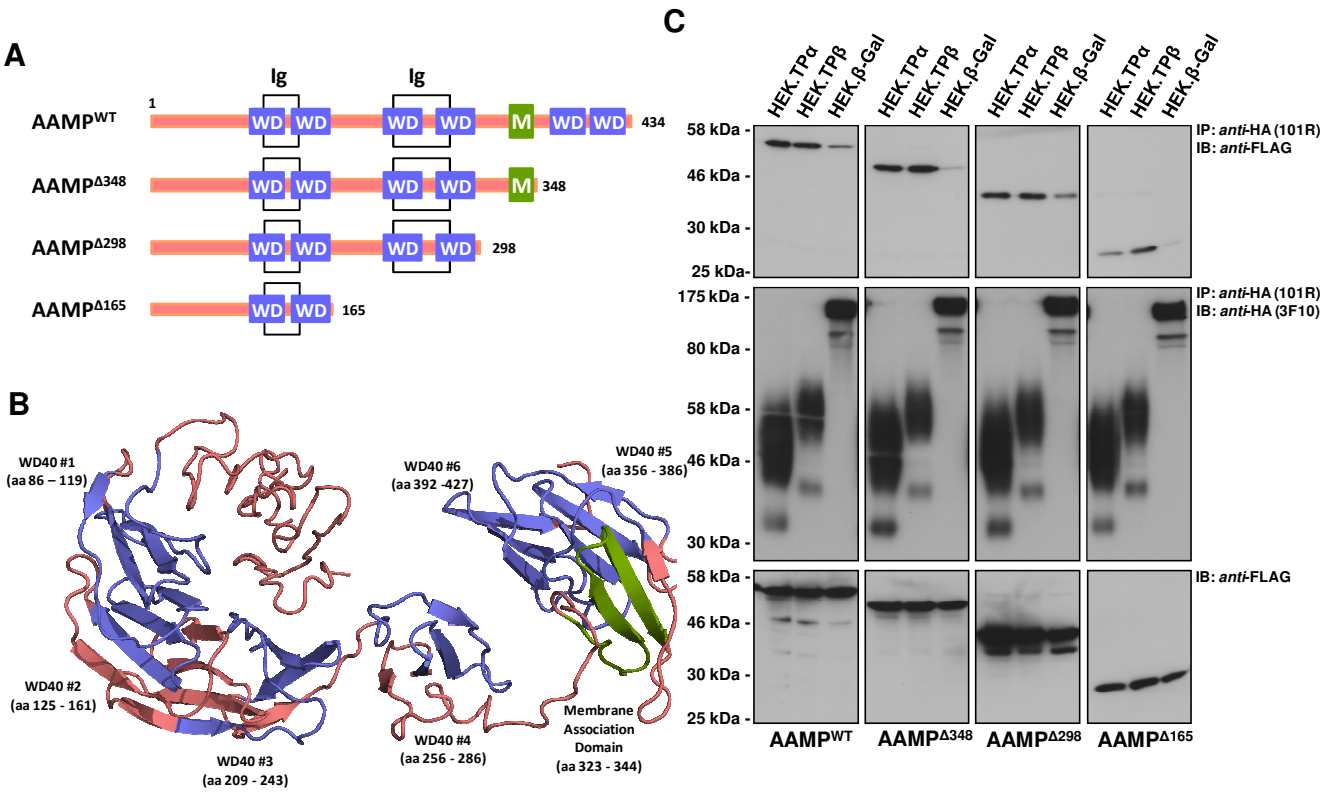

Figure 4. Localization of the regions of AAMP mediating the interaction with TPα and TPβ.
A. Schematic of AAMP highlighting its 6 putative WD-40 domains (blue), 2 immunoglobulin homology domains (white) and a membrane association domain (green). Outlined below are the AAMP subframents generated for this study. B. I-TASSER 3D-structural analysis of AAMP showing the predicted 6 WD-40 repeat domains (blue) and the putative membrane association domain (green). C. HEK.TPα, HEK.TPβ and, as controls, HEK.β-Gal cells were transiently co-transfected with recombinant pCMV-Tag2B vector encoding Flag- tagged-AAMP, AAMP$^{\Delta348}$, AAMP$^{\Delta298}$ orAAMP$^{\Delta165}$ prior to immunoprecipitation with *anti*-HA 101R antibody. Immunoprecipitates (IP) were resolved by SDS-PAGE and were either immunoblotted (IB) versus *anti*-FLAG or *anti*-HA 3F10-HRP conjugated antibody. To verify expression of the AAMP proteins, aliquots of whole cells lysates (~ 50 µg/lane) were immunoblotted with *anti*-FLAG antibody (Lower panels). The relative positions of the molecular size markers (kDa) are indicated. Data; $n \geq 3$.

Figure 5

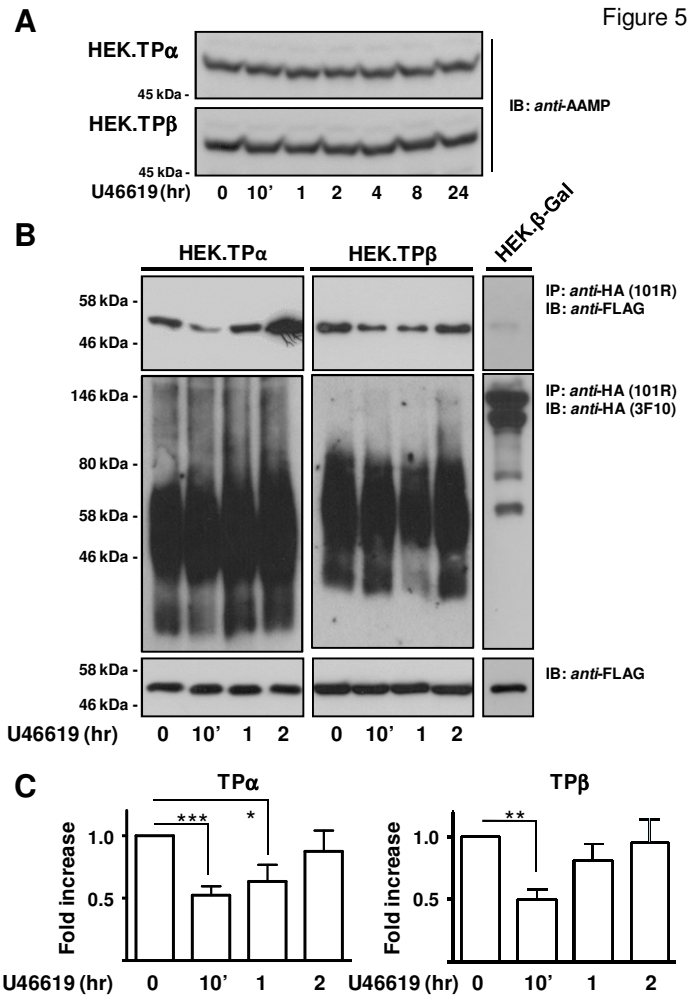

Figure 5. Effect of agonist-activation on the interaction between AAMP with TPα and TPβ.
A. HEK.TPα and HEK.TPβ cells were stimulated with 1 μM U46619 for 0 – 24 hr. Cell lysates (50 μg/lane) were resolved by SDS-PAGE and immunoblotted (IB) with *anti*-AAMP antibody. B. HEK.TPα, HEK.TPβ and, as controls, HEK.β-Gal cells, each transiently co-transfected with pCMVTag2B:AAMP, were stimulated with 1 μM U46619 for 0 – 2 hr prior to immunoprecipitation with *anti*-HA 101R antibody. Immunoprecipitates (IP) were resolved by SDS-PAGE and immunoblotted with *anti*-FLAG or *anti*-HA 3F10-HRP conjugated antibody. To verify AAMP expression, aliquots of the whole cells lysates (~ 50 μg/lane) were immunoblotted with *anti*-FLAG antibody (Lower panels). The relative positions of the molecular size markers (kDa) are indicated. C. Bar charts signify mean fold changes (n = 3, ± S.E.M) in the amount of AAMP associated with the TPα and TPβ immunoprecipitates as a function of U46619-stimulation where basal levels, in the absence of agonist, were assigned a value of 1.0. The asterisks indicate that AAMP levels in *anti*-HA immunoprecipitates from U46619-treated cells were lower than that at 0 hr where *, $p > 0.05$, ** $p > 0.01$ and *** $p > 0.001$.

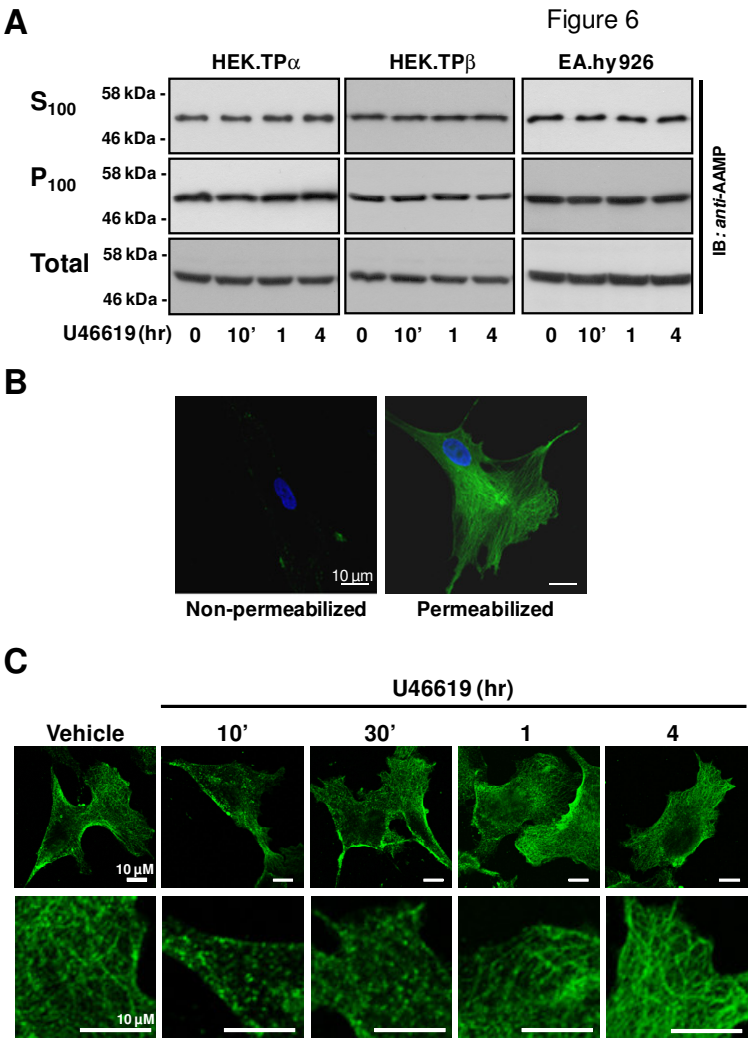

Figure 6. Subcellular localization of AAMP in response to TP agonist treatment.
A. HEK.TPα, HEK.TPβ and EA.hy926 cells were incubated with 1 µM U46619 for 0 – 4 hr prior to fractionation into their soluble (S_{100}) or membrane (P_{100}) fractions. Aliquots (50 µg/lane) of the S_{100}, P_{100} or whole cell lysates (Total) were resolved by SDS-PAGE and immunoblotted (IB) with *anti*-AAMP antibody. Data; n ≥ 3. The relative positions of the molecular size markers (kDa) are indicated. B. 1° hCoASMCs were immunolabelled with *anti*-AAMP antibody under non-permeabilizing or permeabilizing conditions. C. EA.hy 926 cells were pre-incubated with U46619 (1 µM) or, as controls, with the drug vehicle (vehicle) for 0 – 4 hr at 37°C. Thereafter, cells were immunolabelled with *anti*-AAMP antibody under permeabilizing conditions. Images in the upper panels were viewed at 63X magnification and the lower panels represent a further 4 fold-increase in magnification. The horizontal bars in the upper and lower panels represent 10 µm. Data; n ≥ 3.

Figure 7

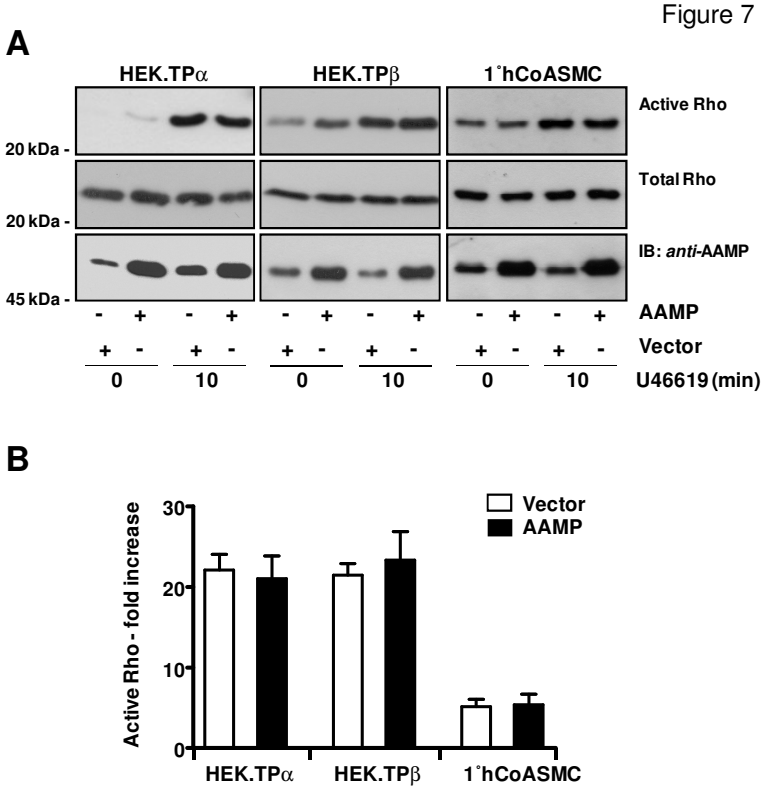

Figure 7. Effect of AAMP on TPα- and TPβ-mediated RhoA activation.
A. HEK.TPα, HEK.TPβ and 1° hCoASM cells were transiently co-transfected with pCMVTag2B:AAMP or pCMVTag2B vector. At 48 hr post-transfection, cells were serum-starved for 5 hr prior to stimulation for 10 min with U46619 (1 μM) or with the drug vehicle. Active Rho was precipitated from the cell lysates using the Rho pull-down assay; resolved by SDS-PAGE and immunoblotted with *anti*-Rho antibody (Upper panels). Aliquots of whole cell lysates were immunoblotted with *anti*-Rho or *anti*-AAMP antibody (Middle & Lower panels). Data; $n \geq 3$. The relative positions of the molecular size markers (kDa) are indicated. B. The bar charts signify mean fold ($n \geq 3$, ± S.E.M) increases in U46619-mediated RhoA activation following transfection with pCMVTag2B:AAMP relative to pCMV-Tag2B where basal levels, in the absence of agonist, were assigned a value of 1.0.

Figure 8

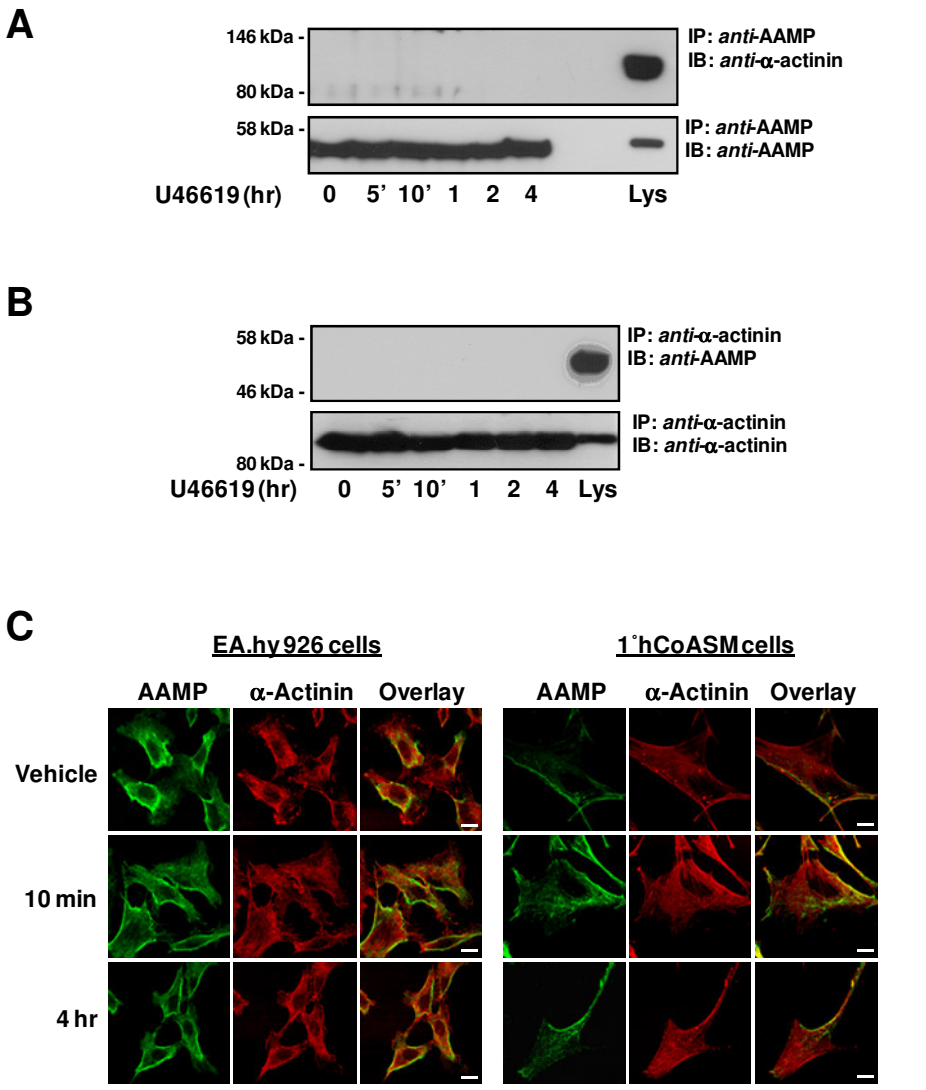

Figure 8. Investigation of a possible interaction between AAMP and α-actinin.
EA.hy926 cells were incubated with 1 μM U46619 for 0 – 4 hr prior to immunoprecipitation with either *anti*-AAMP (Panel A) or *anti*-α-actinin (Panel B) antibody. Immunoprecipitates (IP) were resolved by SDS-PAGE and immunoblotted (IB) with *anti*-α-actinin (Upper panel A) or *anti*-AAMP (Upper panel B) antibody to assess the interaction, and with *anti*-AAMP antibody (Lower panel A) or *anti*- α -actinin antibody (Lower panel B) to confirm precipitation. C. EA.hy 926 and 1° hCoASM cells were pre-incubated with U46619 (1 μM) for 0 – 4 hr at 37°C. Following fixation and permeabilization, cells were immunolabelled with *anti*-AAMP and *anti*-α-actinin antibodies and localized using goat *anti*-rabbit AlexaFluor488 and goat *anti*-mouse AlexaFluor594 secondary antibodies, respectively. Images were viewed at 63X magnification, where the horizontal bars represent 10 μm. Data in all panels; $n \geq 3$.

Figure 9

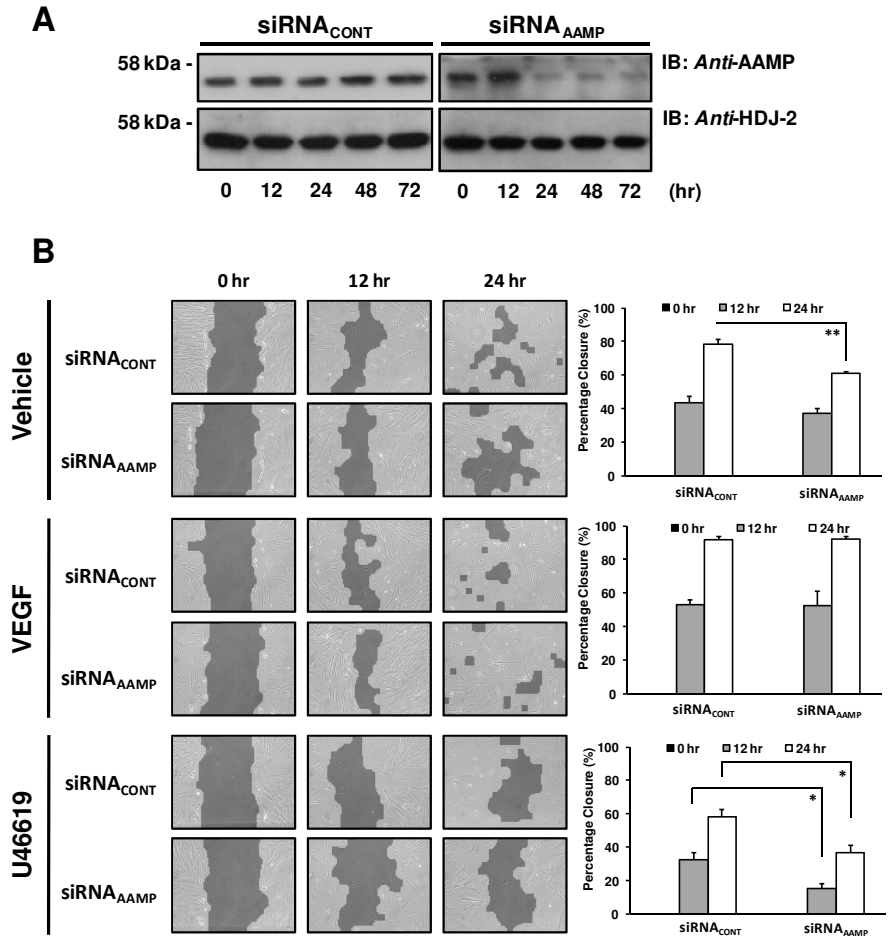

Figure 9. Effect of AAMP on TPα/TPβ-mediated Smooth Muscle Migration.
1^{o} hCoASMCs were transfected with *si*RNA$_{AAMP}$ or the scrambled *si*RNA$_{Control}$. A. Whole cell lysates were resolved by SDS-PAGE and immunoblotted (IB) with *anti*-AAMP and *anti*-HDJ-2 antibody. The relative positions of the molecular size markers (kDa) are indicated. Data; n ≥ 3. B. 1^{o} hCoASMC monolayers were scratched and wounds imaged immediately (0 hr) or following incubation for 12 or 24 hr with 1 μM U46619, 20 ng/μl VEGF or, as control, vehicle (0.01 % EtOH), as indicated. Images were captured using a Nikon TMS inverted microscope with Matrox Intellicam software (version 2.07) and analysed with TScratch software (Version 1.0), where data is presented as mean percentage closure ± S.E.M. Data; n ≥ 3. The asterisks in panel B indicate that migration of 1^{o} hCoASMCs transfected with *si*RNA$_{AAMP}$ is significantly decreased compared to those transfected with *si*RNA$_{Control}$ (*, **, $p > 0.05, 0.01$).

Figure 10

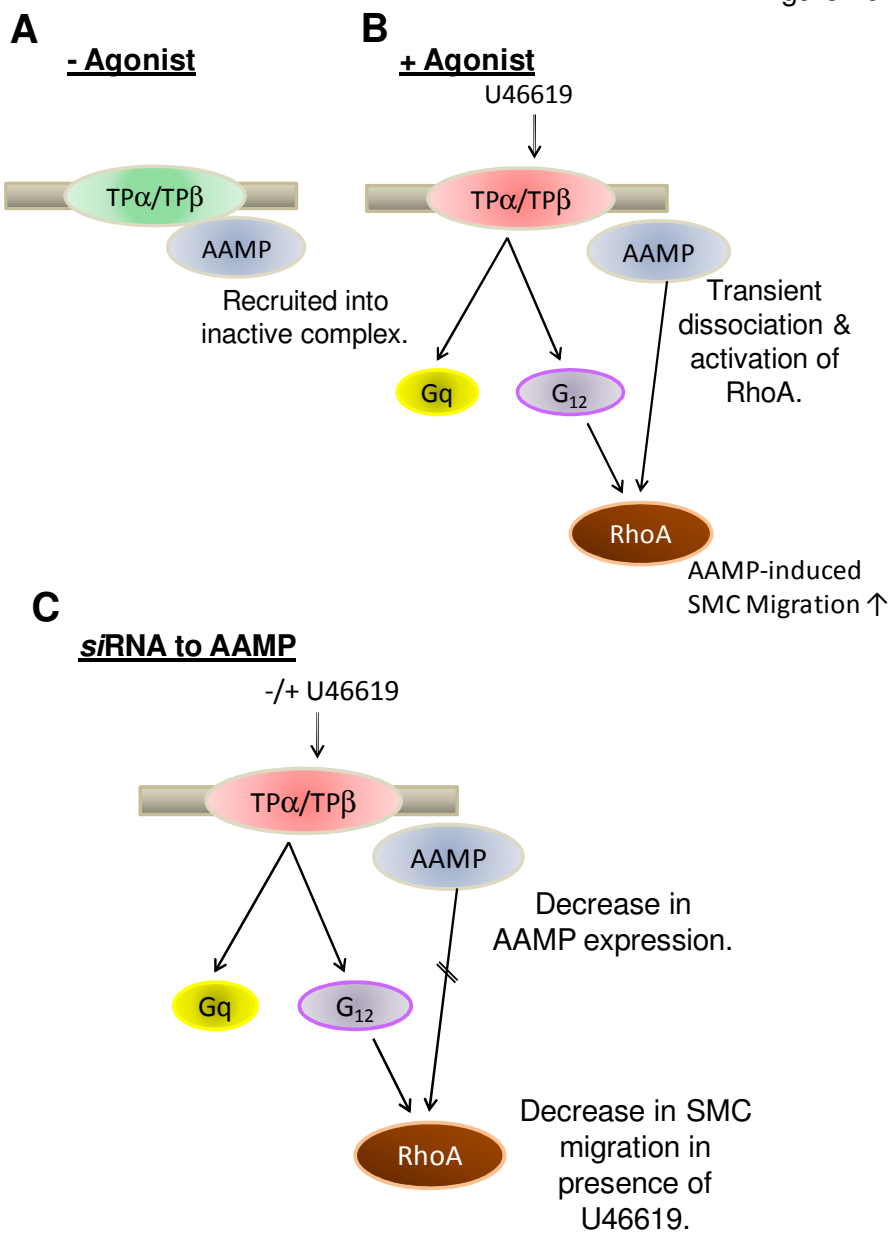

Figure 10. Proposed Model of the Interaction of AAMP with TPα/TPβ.
A. Under basal conditions, in the absence of agonist, AAMP appears to be recruited into an inactive complex with either TPα, TPβ or both. B. In response to U46619-activation, TPα/TPβ are known couple to Gq-mediated activation of phospholipase (PL) Cβ and to G_{12}-mediated activation of RhoA, leading to Ca^{2+}-dependent and Ca^{2+}-independent F-actin polymerization and smooth muscle contraction. Herein it was established that agonist-activation of TPα/TPβ also coincides with a transient dissociation of AAMP from the complex, possibly facilitating AAMP-induced RhoA activation and AAMP-induced SMC migration. C. *si*RNA-mediated disruption of AAMP expression is associated with a decrease in SMC migration in the presence of the TP agonist U46619, but not in the presence of VEGF. Hence, agonist-dependent dissociation and activation of AAMP may be required for any SMC migration that occurs in the presence of TXA_2 or its mimetic U46619.